HEAT TRANSFER EFFECTS

ON A SUBSONIC DELTA WING

by

Raymond William Blohm, III

Thesis submitted to the Graduate Faculty of the

Virginia Polytechnic Institute and State University

In partial fulfillment of the requirements for the degree of

MASTER OF SCIENCE

in

Aerospace Engineering

APPROVED:

J. F. Marchman, III, Chairman

J. A. Schetz

F. H. Lutze, Jr.

July, 1973

Blacksburg, Virginia

ACKNOWLEDGMENTS

The author is grateful to several undergraduate students,

, , and , who assisted in

various phases of the experimental work.

TABLE OF CONTENTS

LIST OF TABLES

LIST OF FIGURES

LIST OF FIGURES - continued

LIST OF FIGURES - continued

NOMENCLATURE

b	wing span, ft.
c	wing chord, ft.
$\bar{c}$	wing mean aerodynamic chord, ft.
C_f	mean skin-friction coefficient
C_ℓ	wing rolling moment coefficient, rolling moment/qSb
C_L	wing lift coefficient, lift/qS.
C_D	wing drag coefficient, drag/qS
C_M	wing pitching moment coefficient about $.25\bar{c}$, moment/$qS\bar{c}$
C_n	wing yawing moment coefficient, yawing moment/qSb
C_p	pressure coefficient, $(p - p_\infty)/q$
C_Y	wing sideforce coefficient, sideforce/qS
M	Mach number
p	pressure
Pr	Prandtl number
q	dynamic pressure, force/area
R	Reynolds number
T	absolute temperature
U	velocity
u	streamwise component of velocity in boundary layer
v	normal component of velocity in boundary layer
x	streamwise spacial coordinate
y	normal spacial coordinate
α	angle of attack, deg.
β	angle of yaw, deg.

NOMENCLATURE - continued

Subscripts

o	total or stagnated conditions
w	conditions at wall
∞	free stream conditions

I. INTRODUCTION

With the space shuttle now being developed, the effects of heating on wings must be studied. During re-entry, the surface temperature of the underside of the wings will reach about 2000°F and peak temperatures on the wing leading edges will reach about 3500°F. However, wing soak temperatures are estimated to be only 1000°R, or 2.5 times local free-stream temperature. Thus, the effects of heating on the aerodynamics and boundary layer of the wing up to this latter range are of critical importance. If the effects are unfavorable, as previous studies have shown for the two-dimensional case, research should be done on defining these effects and the limitations they cause for the vehicle. Then the effects may be designed around or at least minimized.

In the past, many studies have dealt with the reverse case, that of a cooled wall, as it was known that this stabilized the boundary layer and thus delayed separation. However, most of these analytic approaches can also be applied to heated wall cases. An especially good summary of these has been compiled by Macha and Norton.[1] These theories apply only to two dimensional flow.

In the case of swept-back or delta wings operating at incidence, the flow can be highly three-dimensional and these theories no longer apply. For thin wings operating above design angle of attack, such as during approach, holding, and takeoff and landing operations, leading edge separation occurs and vortices appear on the upper surface. These vortices are responsible for large changes in the aerodynamic forces and moments produced by such wings. No work has been found which has

treated the effects of heat transfer on these "bound" vortices.

Therefore, the purpose of the present study is to determine the effects of heat transfer on the forces and flow fields associated with thin delta wings at low speeds.

II. EXPERIMENTAL INVESTIGATION AND TEST PROCEDURE

A simple delta wing planform was chosen for the research for several reasons. First, since the research was to be applicable to the space shuttle, the planform had to be suitable for high-speed flight. As is well known, the rise in drag and change in trim associated with a Mach number approaching unity are postponed to a higher Mach number with increasing sweepback. The delta wing takes advantage of both a large sweepback angle and a small thickness ratio. Further, the displacement of the center of pressure by transition from subsonic to supersonic flight is smaller with a delta planform than a conventional planform. A delta wing also experiences a much less abrupt stall and generates lift to higher angles of attack than conventional planforms. Also, after considerable research, NASA has chosen a double-delta planform for higher efficiency. The decision to remain with a constant sweepback angle was taken both to eliminate the varying sweepback effects (such as on an ogive wing) and to reduce construction costs by means of an available model.

The model was tested in the Virginia Polytechnic Institute and State University's subsonic 6' x 6' stability tunnel. This tunnel is a continuous, single return type with closed test section. It was designed and constructed at the Langley Aeronautical Laboratory of the NACA near Hampton, Virginia, and operated there for fifteen years. The Aerospace Engineering Department acquired the tunnel in 1958 for instructional and research purposes. The tunnel is powered by a 600 hp

dc motor driving a fourteen foot diameter propeller that is capable of producing a dynamic pressure in the test section of 330 lb/ft^2 which corresponds to approximately 350 mph at sea level. The tunnel operates at a turbulence factor of 1.08 due to the presence of seven stainless steel turbulence screens. This value may be compared with the values of 1.01 to 2.67 in comparable tunnels all over the world.

In view of the heat-induced errors which would result from using the strain gauge system, the model was tested on the six-component automatic null balancing mechanical system. The systems feeds its output into a visual indicating dial system and a printer.

The model was strut mounted to the floor of the wind tunnel. An airfoil fairing was mounted to the tunnel floor around the strut to reduce drag and wind forces on the strut.

The wing was a symmetrical, 60° sweepback, delta wing with a modified double wedge section. It was cast in aluminum from a delta wing that had been used in previous NACA tests in the VPI&SU tunnel before transferral. The wing characteristics are summarized in Tables 1 and 2 and a sketch of the wing is shown in Figure 1.

The decision was made to make the model a one-piece homogeneous wing to minimize the effects of thermal expansion and wing warpage. This also made the imbedding of heating elements in the model undesirable. Instead, an external infrared heating source was used. One 40,000 btu/hr and two 15,000 btu/hr infrared burners were arranged in a triangular pattern on a circular base plate with a semicircular wind shield. The base plate was adjustable in pitch, yaw, and vertical

distance to maintain a constant heating pattern over the delta wing. The base plate was fully retractable through the top of the wind tunnel with a self-actuated door then sealing the tunnel opening. The base plate and burners are shown in an extended position in Figures 2 and 3 and in a retracted position on top of the tunnel in Figure 4.

The right side of the delta wing was instrumented with ten thermocouples mounted along the leading edge, the center section, and along a line through the mid-chords of the wing. These thermocouples were connected to a digital readout and a strip chart recorder. The experimental test instrumentation and wind tunnel controls are shown in Figure 5.

The model was first tested in an unheated mode to provide base-point data. This also provided data that could be compared with previous NACA data on the same wing. Six component data was obtained for an angle of attack range of 0° to 36° in two degree increments through 26° and one degree increments thereafter. Yaw settings were -10°, -6°, -2°, 0°, +2°, +6°, and +10°. The wind tunnel was operated at a velocity of 148 fps, corresponding to a Reynolds number of 1.60×10^6.

Flow visualization studies were then conducted with tuft patterns and oil flows on the model to understand the basic flow patterns. The same angle of attack range and yaw settings of -10°, -6°, 0°, +6°, and +10° were studied. Photographs were taken and are shown in Figures 6-37.

The heated portion of the tests were conducted as follows. The model was set to the required pitch and yaw settings, and the base

plate heater lowered and ignited. Upon reaching the desired temperature, the plate and doors were retracted and the tunnel brought up to speed simultaneously. After the flow and balance system reached equilibrium, readings were taken every 5-10 seconds. By means of an event recorder on the strip chart recorder, it was possible to fix the exact temperature at each balance reading. Due to only one strip chart recorder channel being available for the testing, a selector switch was used in preliminary heated tests to determine which thermocouple location provided the mean temperature reading of the group. This location (at the center section 33% chord) was then used in all succeeding tests. Temperature readings were taken at all ten stations at the beginning and end of each test. Angle of attack and yaw settings were the same as those of the visualization studies. Heated tests at zero yaw angles were run three times for verification. It should be noted that the ambient reference temperature used in calculating the wall temperature ratios was 65° F, which corresponds to the average wind tunnel test section temperature.

III. LITERATURE REVIEW AND THEORETICAL INVESTIGATION

Unheated Wing Analysis

In order to fully understand the changes in flow pattern over the delta wing due to heat transfer, it is felt that first flow over the unheated wing must be completely understood. Therefore, the unheated wing analysis is divided into two sections. The first section explains the generalized flow pattern over a delta wing. The second section treats the parameters that affect flow over a delta wing. Finally, the third and fourth sections summarize research into two- and three-dimensional heat transfer.

Generalized Flow Pattern

The generalized flow pattern over a delta wing at incidence will be summarized with Figure 38 as guide, following Sutton.[2] At some point along the leading edge, the boundary layer separates and forms a part-span vortex sheet, the unbound edge of which rolls up above the wing's upper surface. Freestream air is forced upward and over the vortex sheet and then swept down toward the wing surface again. There exists a dividing streamline separating the vortex-entrained inner flow from that flow further outwards not entrained. Streamlines which become entrained in the vortex flow under the vortex sheet with a large spanwise velocity component and continue spirally downstream into the core of high vorticity formed by the rolling-up of the edge of the sheet. Streamlines which pass above the dividing streamline

continue downstream over the wing inboard of the vortex sheet in an approximately chordwise direction.

Underneath the vortex core formed by the rolled-up edge of the part-span vortex sheet, the local suction is large on the wing surface. The new boundary layer formed by the outward surface flow encounters an adverse pressure gradient after passing the suction peak and separates before it reaches the leading edge. The area under the main vortex sheet near the leading edge may contain a secondary coiled vortex sheet, or more probably a separation bubble of relatively slow-moving air.

At moderate angles of attack, the part-span vortex sheet is roughly conical in shape above the wing, with the apex on the leading edge. The rolled-up edge of the sheet stays close to the wing surface along a ray from its apex, lying in plan view between the leading edge and a line through its apex in the freestream direction. The presence of the part-span vortex sheet is advantageous in that it effectively limits the rearward extension (in the freestream direction) of the separated region over the sections for a small distance outboard of the origin of the vortex sheet. In addition, the part-span vortex creates more local lift in that area than that which is lost through the leading edge separation. At higher angles of attack, the vortex core may lift farther away from the wing surface well ahead of the trailing edge, and trail downstream more nearly in the freestream direction. The chordwise position at which this happens moves forward as the incidence increases. Also, vortex breakdown may occur.

At these high incidences, the flow separation is at the leading edges except possibly for sections close to the wing root, where turbulent separation from the rear may occur first.

As the angle of attack is increased, separation will occur near the wing tip first, or at least at a section further out along the span than the position for the maximum in the spanwise distribution of C_L, for two reasons. The first reason is the spanwise variation in the shape of the chordwise loading. Near mid-semi-span, the chordwise loading is similar in shape to that on an airfoil in two-dimensional flow, but near the wing tip the loading is changed such that the peak suction on the upper surface for a given local C_L occurs nearer the leading edge and is greater in magnitude. Second, the wing taper causes a smaller local Reynolds number near the wing tip due to chord variations. This is important when the local C_L at which separation first occurs is varying rapidly with Reynolds number.

In the same manner, as the leading edge of the separation--and thus the origin of the vortex sheet--approaches the wing root leading edge with increasing incidence, the forward movement slows as the wing root is approached. Rephrased, the flow near the wing root leading edge reaches an appreciably higher local C_L than the leading edges of sections further outboard before separating. This delay in separation at the wing root leading edge is for the same reason as the quick separation at the wing tip leading edge, i.e., near the wing root the chordwise loading is changed such that the peak suction

on the upper surface for a given local C_L occurs further back from the leading edge and is smaller in magnitude than on the sections further out on the wing.

Flow Parameters

In the case of an unheated delta wing, there are five parameters which modify the flow: (1) Reynolds number, (2) surface condition, (3) freestream turbulence, (4) leading edge radius, and (5) sweepback. Of these parameters, the first three barely affect the surface pressures near the leading edge in the absence of separation, but may change the development of turbulence in the boundary layer. Thus, these "viscous" parameters will influence the occurrence of separation and the development of the part-span vortex sheet.

Increasing Reynolds number effectively reduces the part-span vortex sheet through increased turbulence. It should be noted that boundary layer transition is an increasingly stabilizing factor with regards to separation, thus inhibiting the formation of the vortex sheet. However, at high incidences, a cross flow mechanism may cause an incipient vortex layer while transition is incomplete. Garner and Bryer[3] found that at very low Reynolds numbers of 0.4×10^6 and below, the vortex sheet and the inboard separation bubble seemed to merge. Here turbulence developed slowly so that the vortex sheet developed easily and merged with the extensive laminar-separation bubble. For moderate Reynolds numbers of 0.9×10^6 to 2.0×10^6, the origin of the vortex became more distinct and was shifted further

toward the wing tip along the leading edge. Also, the vortex pivoted to a more chordwise direction. Thus, at larger Reynolds numbers, the greater diffusion of turbulence restricted the size of the vortex layer. In addition, increased Reynolds number also encourages reattachment due to reduced boundary layer thickness.

Surface condition also affects vortex formation due to development of turbulence. Limited surface roughness at the leading edge is effective in producing a forward transition at low incidence and thus hindering the occurrence of the vortex sheet. However, for increased velocity, and thus Reynolds number, this same surface roughness may cause a more extensive vortex sheet due to turbulent separation over the whole roughened surface.

Stream turbulence is important due to the increasing stabilization of transition. Garner and Bryer reported a progressive chordwise delay in vortex formation with increasing stream turbulence. For an intensity of freestream turbulence of 0.1 per cent, they reported that a smooth wing experienced laminar growth up to separation with turbulent diffusion still in progress as the vortex originated. However, for an intensity of about 1 per cent the turbulent diffusion was more advanced so that transitional reattachment occurred before vortex formation. Also, they reported a delayed inwards progress of the vortex with increasing incidence in high freestream turbulence. Thus, stream turbulence is clearly as important a parameter as Reynolds number.

The last two parameters--leading edge radius and sweepback--

unlike the first three vitally modify the pressure distribution in all circumstances.

The leading edge radius strongly influences the extent of the vortex sheet. Where the leading edge is sharp, the boundary layer separates along the entire leading edge so that the vortex originates from the leading edge wing root. For a rounded leading edge, when the leading edge radius is reduced so that suction peaks are higher and higher, it is known that for a given incidence the vortex sheet is of a greater spanwise extent.

The primary effects of sweepback pertinent to this paper are due to the effects of yaw on the relative incidence of each leading edge to the freestream. A rotation of ten degrees on a wing with 60° sweepback has been shown[3] to cause the vortex origin to shift toward the wing root and to align the vortex closer to the leading edge for the more swept-back side. Also, two separation lines appear, one close to the leading edge and the other small and inboard of the vortex. These lines are first seen close to the vortex origin and lengthen with increasing yaw. The inboard separation line is due to the boundary layer separating along the line and rolling up to form a weak vortex, which is subsequently entrained in the part-span vortex. Thus, an increase in the leading edge sweep causes a reorganization of the part-span vortex sheet. This is probably due to the action of a cross-flow mechanism resulting from the increased spanwise component of velocity. Garner and Bryer found that this mechanism of flow began to operate when the leading edge sweep was approximately 55°

and continued with increasing effectiveness at the higher angles of sweep.

Both Elle[4] and Earnshaw[5] have shown how the leading edge sweep angle is a dominant parameter in determining the breakdown location of vortices. Elle showed that for some given incidence, the breakdown location for vortices was almost the same for edges of equal sweep whether this sweep was obtained by an unyawed model or a yawed wing of smaller apex angle.

Two-Dimensional Qualitative Conclusions

The theoretical study of heat transfer on wings received much attention in the post World War II to 1960 period, then remained quiescent until the advent of the space shuttle produced a revival. Much of this work was oriented towards stabilization of the boundary layer through cooling the surface, but is applicable to this study. The following qualitative conclusions for two-dimensional flows have been reached by previous investigators.[1,6-14]

1. A heated surface increases the velocity boundary layer thickness.
2. A heated surface decreases the velocity at a fixed point within the boundary layer.
3. A heated surface increases the direct effect of a given pressure gradient.
4. A heated surface's effect on skin friction depends on the nature of the pressure gradient.

a. In an adverse pressure gradient, the dynamic and viscosity effects tend to magnify each other, decreasing the local skin friction.

b. In a favorable pressure gradient, the dynamic and viscosity effects oppose each other, allowing no qualitative conclusions.

5. A heated surface causes the point of separation in both laminar and turbulent flow to move upstream.

6. A heated surface destabilizes the boundary layer, moving the transition region upstream.

These two-dimensional conclusions relate directly to the aerodynamic efficiency of a wing. By increasing the velocity boundary layer thickness and effectively increasing the direct effect of an adverse pressure gradient, a heated wing surface will tend to shift the point of separation on a wing upstream. Even if there is only a small increase in separation (approximately 5% of the chord), the drag force will be increased due to the wider wake and corresponding larger region of pressure loss. At the higher angles of attack, this increasing separation due to a heated wing surface will cause a direct reduction in maximum lift and an earlier stall. The tendence of a heated surface to destabilize the boundary layer and move the transition region upstream would have a direct effect on the cruise efficiency of the wing. In the absence of separation, an increased area of turbulent flow due to heating will cause an increase in drag at cruise and reduce the maximum range of the vehicle.

It is felt that in view of the availability and much more detailed treatment given in the original papers, very little of the analytical derivations contained there will be presented in this paper. Instead, a summary of the methods used, the assumptions made, and the conclusions reached will be presented.

In one classic paper on compressible laminar flow, Van Driest[6] uses the Crocco method of transforming the independent variables x and y into x and u, where $u = f(x,y)$. By substitution of the shear stress equation into the basic equations and elimination of terms by subtraction, two equations are derived as functions of x and u. The basic assumptions to this point are that of two-dimensional steady flow over a smooth flat plate with constant Prandtl number. To solve the equations, the enthalpy is assumed to be a function only of the velocity (corresponding to a Prandtl number of one), and a basic viscosity-temperature law (power or Sutherland) is assumed. Some results of this report are shown in Figures 39-41.[6] It is shown in Figure 39 how increasing the wall temperature actually decreases the mean skin-friction coefficient in the absence of a pressure gradient. Figure 40 presents the velocity distribution in a boundary layer with varying wall temperatures. It can be seen that heating the surface decreases the velocity at a fixed point within the boundary layer. Alternatively, this may be viewed as increasing the velocity boundary layer thickness with heating. Similarly, Figure 41 shows how the temperature boundary layer thickness is increased with heating, as is intuitively expected.

Another classic series of papers by Morduchow, et al. is representative of this period when integral methods were dominant.[7-12] Libby, Morduchow, and Bloom conducted an investigation into the relative merits of the various integral methods.[7] It was concluded that in general the one-parameter method based on the Kármán momentum integral equation in conjunction with a sixth-degree velocity profile was superior. After this, Morduchow and Clarke derived a method of calculation, including separation and stability, for flows with a pressure gradient but no wall heat transfer.[8] It was also shown that fourth-degree profiles are optimal for stagnation flows, and similarly seventh-degree profiles for the separation point in an adverse pressure gradient. This was later expanded by Bloom to flow with heat transfer, and the use of sixth-degree profiles for stability calculations on a flat plate was developed.[9] Libby and Morduchow later expanded this to flow with a pressure gradient.[10] Morduchow and Grape then published a general study of all the previous effects.[11] Finally, Morduchow summarized previous work and extended it to non-isothermal surfaces.[12]

In general, the same assumptions are used as in the Van Driest paper. An ideal-gas law is again assumed. It is assumed that c_p and c_v are constants, and that the Prandtl number is constant and of the order one. The continuity equation is multiplied by u and added to the energy equation. The viscosity-temperature relation is approximated by the Sutherland Law. Because this includes compressible flow, the Dorodnitzyn transformation is used, replacing the physical normal

coordinate. The velocity and stagnation-enthalpy profiles are chosen as sixth and seventh degree polynomials. By assuming a Prandtl number of one and constant wall temperature, the velocity and energy boundary layer equations can be integrated to two integrodifferential equations, which by substituting in the polynomials are reduced to two ordinary differential equations in two unknowns.

The authors have shown that the effect of the wall temperature on the various parameters arises from two areas. First, the conditions of dynamic equilibrium, as defined mathematically by the basic differential equations and their solutions. Secondly, by the variation of the viscosity coefficient with temperature, as defined mathematically by the constant (which includes the wall temperature) in the Sutherland Law.

Under the first area, the effect of the wall temperature depends on the nature (adverse or favorable) of the pressure gradient. Without the effect of the second area, raising the wall temperature in a favorable pressure gradient tends to increase the local Nusselt number and especially the local skin friction. In an adverse pressure gradient, the Nusselt number and especially the skin friction are decreased.

Both the Nusselt number and the local skin friction are also functions of the viscosity coefficient. However, the viscosity coefficient is contrary to the dynamical effect, independent of the pressure gradient. Thus, when the wall temperature is increased and is greater than 216°R, the Nusselt number and skin friction are

decreased. (The reverse is true for a wall temperature increased but less than 216°R, but is not a factor in the present case.)

Thus, depending on the nature of the pressure gradient, the dynamical and viscosity effects of the wall temperature may tend either to magnify or to partly cancel each other. In the present case, these effects will tend to oppose each other in a favorable pressure gradient and to magnify each other in an adverse pressure gradient.

A second significant effect can be observed from raising the wall temperature. It can be inferred from the basic equations that raising the wall temperature has a tendency to magnify the direct effect of a given pressure gradient. This is important in laminar separation.

By differentiating the momentum partial differential equation of the laminar boundary layer, it can be shown that under the present assumptions of a Prandtl number of one and a linear viscosity-temperature relation,

$$\left.\frac{\partial^4 u}{\partial y^4}\right|_w = 0$$

at a separation point with or without heat transfer at a wall.[8] A seventh-degree velocity profile is then chosen to satisfy the preceding equation as well as the boundary conditions satisfied by the sixth-degree profiles in the preceding analysis. Equations are then worked out giving the position and the boundary layer thickness at separation.

With respect to the effect of the wall temperature on the separation point, it is seen from the equations that the separation point is independent of the viscosity coefficient. Thus the viscosity-temperature relation, as it is incorporated in the viscosity coefficient, does not have the significant effect on the separation point that it has on the Nusselt number and skin friction. The effect of wall temperature on the separation point will thus arise only from its dynamical, or pressure gradient, effect. The equations imply that raising the wall temperature will have an unfavorable effect on separation by moving the separation point upstream. This hastening of separation caused by heating of the wall is an illustration of the general tendency remarked on earlier for an increase in the wall temperature to increase the direct influence of a pressure gradient. Figure 42 shows this effect.[11]

Morduchow and Grape also determined the effect of wall temperature on flow stability characteristics.[11] The minimum critical Reynolds number at a given station was calculated as a function of the wall temperature. The stability criteria as developed by Lin and Lees and used in reference 11 are based on the amplification or decay of small disturbances, and the minimum critical Reynolds number thereby obtained is the minimum Reynolds number required for the possibility that at least certain types of disturbances will be amplified. Thus, the existence of a Reynolds number exceeding the minimum critical Reynolds number is a necessary condition for instability of the laminar boundary layer. It can thus be qualitatively concluded that the higher the

minimum critical Reynolds number, the more stable the flow and the less the tendency for transition. Morduchow and Grape found that heating the wall had a destabilizing effect on the boundary layer, since the minimum critical Reynolds number decreased as the wall temperature ratio was increased.

A recent survey and experimental paper by Macha and Norton[1] used the integral relation method of Walz[13] and the finite-difference, eddy conductivity, eddy viscosity method of Cebici, Smith, and Wang[14] to investigate the effect of a heated wall on the location of the point of separation in turbulent flow. Both methods, as shown in Figure 43 (Ref. 1), though differing in the location of the separation point agree in the magnitude of the upstream movement of the separation point with increasing wall temperature.

Three-Dimensional Qualitative Conclusions

At the time of this writing, very few papers are available on the effects of heating on three-dimensional flow in general, and particularly on vortices. Recently, a few papers have been published on the accelerated breakdown of aircraft trailing vortices with heating. It is understood that there are many differences between a free trailing vortex and a vortex sheet on a wing surface, but it is felt that enough simularities exist to draw qualitative conclusions. Sutton[2] draws the following conclusions about a vortex sheet: "A part-span vortex layer includes an 'outer stratum' of high shear and maximum turbulent energy, where the main stream coalesces with the

strong inflow above the 'vortex core'; the core, itself of low energy, lies about midway between the 'outer stratum' and the wing surface. The use of the expression 'vortex core' is justified by the fact that a superimposed potential vortex of the given strength so situated would roughly reproduce the experimental surface pressures." Thus, a vortex sheet has a core and an outer region.

Mironer describes the effects of heating on the vorticity diffusion rate in a vortex.[15] It is seen that heating causes increased diffusion only in a vortex having an initially cold core and hot outer region. This is the case in the vortex sheets where air passing over the vortex core is swept down again close to the heated wing surface and heated, then swept in a spiral pattern around the vortex core. If the vortex is in a compressible medium and the vortex core is initially cooler than the outside induced region, a radial velocity is generated which convects mass out of the vortex core (density decreasing) into the outer regions which are being cooled (density increasing). Thus, a radially outward convection of mass as well as vorticity is generated. This supplements the pure outward diffusion of vorticity. In addition, the increased kinematic viscosity in the high-temperature, low-density regions increases the pure Fourier rate of vorticity diffusion. It was found that a temperature ratio of 2.0 across the vortex nearly doubled the vorticity diffusion rate over that of a vortex with no heating.

In a later paper, Costen also examined the question of whether heat addition could result in more rapid dissipation of the trailing

vortices.[16] It was found that more heat was required than was available from the engines of a jet transport.

As a result of the latter paper, it is felt that the heat supplied by the wing at a wall temperature ratio of 2.0 to the outer vortex layers is not sufficient to cause a significantly more rapid dissipation of the vortex sheets. It is also felt that the actual temperature ratio of the outer layers is far below 2.0 due to the continual addition of new cold air to the vortex sheet from the surrounding flow.

IV. RESULTS AND DISCUSSION

Unheated Wing Analysis

The flow pattern of an unheated delta wing is highly complex, so it was necessary to analyze the normal unheated flowfield before a valid heated analysis could be made. The wing was tested at angles of attack up to 36° and angles of sideslip between +10° and -10°. Flow visualization studies were conducted with oilflow and tuft patterns.

The tests were conducted at a Reynolds number of 1.60×10^6 based on the mean aerodynamic chord. This is in the range of increased turbulence and thus partial vortex sheet restriction. The surface condition was relatively smooth except for the aforementioned casting defects. These were too random to predict surface roughness effects. The turbulence factor of 1.08 is quite low for wind tunnels, thus tending toward transitional reattachment at low angles of attack. The leading edge was rounded so that the vortex did not originate over the whole leading edge at once. This rounding made it impossible to use the Polhamus leading-edge suction analogy theory, but this theory becomes inaccurate when leading edge sweep approaches 60°, regardless. This is probably due to the action of the cross-flow mechanism described earlier.

In the following, the oilflow and tuft studies, Figures 6 through 37, are used to build up a picture of the flow with increasing incidence. Oilflow patterns are employed to visualize the primary and secondary separation lines, while the tuft patterns locate the reattachment of the leading edge vortex sheet. The latter is marked by an abrupt

change in direction of the tufts. The variations of lift, drag, and pitching moment with angle of attack at zero yaw are shown in Figures 44-46. This data agreed with the previous NACA data recorded in the tunnel.

At an incidence of 0°, the streamlines were straight and there was no spanwise flow except on the outer quarter of the wing semi-span. It is believed that due to the flow parameters previously cited, the transition to turbulence was early.

At an incidence of 4°, there appeared a leading edge separation with turbulent reattachment along most of the leading edge. From the small herringbone strip, it appeared that the formation of the part-span vortex sheet was imminent. Inboard of the separation, there was little or no spanwise flow.

Between the angles of 4° and 8°, the leading edge separation became more pronounced and gave rise to the vortex sheet. By an incidence of 8°, the vortex sheet had reached about four-fifths of the way to the wing root leading edge. Note that due to the distortion of the wing loading at the wing tip previously mentioned, there were small separation bubbles at the leading edges of the wing tips. There was now noticeable spanwise flow on the outer third of the semi-span.

The force measurements first showed a reduction in stability between the angles of 12° and 14°. It has been shown that the main effects that a vortex sheet has on the loading of the wing are an increase in lift beneath the rolled up edge and a loss of lift further outboard. Since by an incidence of 14° the aerodynamic center was

beginning to move forward without any measureable change in the lift-curve slope, it is seen that the loss of lift at the wint tips must have been balanced in magnitude by the gain in lift acting further forward beneath the rolled up edge of the vortex sheet.

By an incidence of 16°, the origin of the vortex sheet had almost reached the wing root leading edge. The separation bubble had grown and lengthened considerably. The dividing line between the vortex and the streamwise flow curved and became less distinct on the rear third of the wing. This was probably due to the vortex core lifting further away from the wing surface in this area, because of the increasing influence of the trailing edge on the otherwise roughly conical development of the vortex sheet. The aerodynamic center continued to move forward between 14° and 16°. The loss of lift over the outer part of the wing trailing edge as the vortex core lifted off may have caused this further decrease in stability, but the increase in lift on the forward part of the wing due to the movement of the origin of the vortex sheet close to the root leading edge was probably of greater effect.

Between 18° and 20° the vortex origin reached the root leading edge. A recovery of stability was seen due to both the vortex origin reaching the root and thus not being able to move forward with increasing incidence affecting increasing detachment of the vortex core from the rear part of the wing.

With further increase in incidence, the point at which the dividing line became indistinct now moved forward. At the same time, the whole surface flow pattern due to the vortex sheet moved inboard,

turning about the root leading edge. Between 22° and 24° the lift lost by root leading edge separation began to approach that gained under the vortex, so the lift-curve slope began to decrease. Finally at 33° the loss exceeded the gain and the net lift began to decrease. It was seen that there was no turbulent separation from the rear at incidences up to 36°, although from the streamlines at 36° it appeared such a separation beneath the vortices was near.

Haines notes how it is possible to deduce the pattern of separation without photographs by the variation of C_D with C_L^2. [17] When a region of separated flow first appears, the rate of increase of C_D with C_L^2 should be markedly increased. This occurred between the angles of 10° and 14°, as shown in Figure 47, thus agreeing with the photographic analysis. Furthermore, this variation should increase even more rapidly when the vortex sheet has ceased to restrict the rearward extension of the separation bubble. This occurred between 27° and 29° and is shown by the photographs to be the result of the vortex core lifting off the rear surface and possibly breaking down.

Significant changes in the flow pattern were evident for variations in yaw. At an angle of attack of 8°, yawing the wing produced two separation lines on the effectively less swept side as previously mentioned. The inboard line moved slightly further toward the wing tip with a decrease in effective sweep. The weak vortex springing from this separation appeared effective in reducing the extent of the part-span vortex sheet outboard of the separation line. On the side with effectively greater sweep, the vortex origin moved slightly toward the root leading edge and pivoted outboard slightly around the apex.

At the higher angles of attack, even a slight yaw produced large separated flow regions on the less swept side, indicating that a major reorganization of the flow occurs at a sweep of 55°-60°. It was seen that even a yaw of 6°, effectively reducing the sweep to 54° on the upwind side, caused large separation even at moderate angles of attack. Ultimately, at a yaw of 10° and high angles of attack, no vortex was visible on the surface of the upwind side at all. On the side with effectively greater sweep, no reorganization was present and the vortex continued its trend of moving the origin towards the apex and pivoting outwards.

Six-component force and moment data are shown as functions of the angle of yaw in Figures 48 through 53.

Heated Wing Analysis

The heated tests produced two facts that largely determined the pattern of the results. First, the origins of the vortices and the structure of the vortex sheets were not affected significantly by wall temperatures in the range of this paper. Secondly, the vortex sheets were extremely dominant in determining the aerodynamic and boundary layer characteristics of the wing. Unfortunately, no visualization studies could be done on the hot wing, so results had to be interpreted from the force and moment measurements taken in the tests.

The zero-yaw lift forces, as shown in Figure 54, show the influence of the vortices. The effect of temperature on the lift was practically nil. There was no decrease in stall angle of attack. A very small but

consistent loss of lift with increasing temperature on the order of a ΔC_L of 0.01 was observed in the data between angles of attack of 24° and 33°. It should be noted that this is within the magnitude of error of the balance system, but due to the consistency of the pattern, it was included in the report. It is in this angle of attack range that the vortex effect on lift and separation is most dominant. Thus, the effective lack of change in lift with temperature shows that the vortex is not significantly affected, since a small change in vortex strength or location would have a large effect on lift. The small decrease in lift is thought to be due to turbulent separation from the rear in the central area between the two vortex sheets. This is the area least affected by the sheets, and it was seen earlier that increasing wall temperatures cause forward movement of the turbulent separation point in two-dimensional flow due to increasing the direct effect of the adverse pressure gradient. This effect, in combination with both the increasingly adverse pressure gradient due to pitch and the weakening vortex influence, is felt to cause a separation in this area. It will be analyzed in detail along with the drag data.

The zero-yaw drag forces, as shown in Figure 55, showed a strong temperature dependence. The first indication of drag increase occurred at an angle of attack of 10° and a wall temperature ratio of 1.95. As the angle of attack increased, the first drag increase occurred at progressively lower temperature ratios until at an angle of attack of 36° it was at 1.2. At the stall angle of 33° (as defined by the point where maximum lift occurs), the first drag increase occurred at a wall

temperature ratio of 1.4. In the previously mentioned angle of attack range of 24° to 33°, the drag increased by 8 per cent to 12 per cent at a wall temperature ratio of 1.8 and, through extrapolation, 15 per cent to 25 per cent at a ratio of 2.0. The mechanism responsible for this increase is that which was mentioned earlier, i.e., a turbulent separation from the rear. To understand this, the flow field in the neighborhood of the wing, not just at the surface, must be considered. The minimum pressure in the neighborhood of the vortex sheet, and thus the maximum lift, occurs on a line whose projection on the wing is near the center of the vortex sheet. However, in the side view the distance between this line and the wing surface steadily increases as the trailing edge is approached. Thus, the influence of the vortex sheet on the surface pressure distribution should decrease towards the trailing edge. Eventually, the effect of the increasing distance between this line and the wing surface with increasing incidence will more than counteract the effect of the increased strength of the sheet with increasing incidence, and the influence of the sheet on the wing surface will decrease markedly. The possibility of vortex breakdown moving upstream over the trailing edge with increasing incidence would produce the same effect. At the same time, the adverse pressure gradient effect is increasing with incidence. When the aforementioned heating effect adds to these factors, a turbulent separation near the rear of the root will eventually occur and ultimately there may be no attached boundary layer aft of the vortex sheet.

The temperature ratio required to increase drag may thus be used as a measure of the onset of separation in the turbulent boundary layer of this region. Thus, at an angle of attack of 10°, there was no tendency towards separation and a high temperature was needed to bring about a small separation. By 22°, the flow would have separated without the effect of the vortices, but with the vortices the flow was still stable until a temperature ratio of 1.7. The effect of the vortices gradually diminished as they lifted away from the surface with incidence, allowing easier separation with incidence. Finally, at angles at and above stall, the unheated flow in the rear root sections was on the verge of separation as can be seen from the small amount of heat addition necessary to cause separation and increased drag.

Further evidence of the rear separation can be seen in the zero-yaw pitching data, as shown in Figure 56. A small decrease in stability, on the order of 5 per cent to 10 per cent, is caused by an increase in wall temperature ratio to 1.8 in the angle of attack range over 22°. This would be explained by a small loss of lift at the rear of the wing as previously mentioned.

Yaw and roll moments were not affected by heating, thus showing a symmetry of heating effects.

The relationship between lift and drag is important in vehicles like the space shuttle. Therefore, a polar diagram is shown in Figures 57 and 58. It can be seen that temperature effects are minimal in all cases below a lift coefficient of 0.8. At a wall

temperature ratio of 1.4, they were only effective above the stall. However, at a ratio of 1.6, a small penalty was being paid in drag for lift coefficients between 0.9 and 1.1. By a ratio of 1.8, the penalty was much greater over the same range.

The effects of temperature in yaw or sideslip were similar to that for zero yaw. Again, the temperature effects on lift were practically negligible. Pitching moment data were also slightly less stable with increasing temperature. However, as shown in Figures 59 and 60, there were greater drag increases with temperature increases and these increases occurred initially at lower temperature ratios. At a yaw of +6°, the drag increased in the 24° to 32° angle of attack range by 10 per cent to 15 per cent at a wall temperature ratio of 1.8 and, through extrapolation, 18 per cent to 25 per cent at a ratio of 2.0. By a yaw of +10°, the drag increased by 25 per cent to 35 per cent at a ratio of 1.8 and, through extrapolation, 40 per cent to 48 per cent at a ratio of 2.0. Also, the drag data at an angle of attack of 8° and 0° yaw yielded no increase through a wall temperature ratio of 1.93. At 6° yaw, the drag began to increase at a ratio of 1.87, and by a yaw of 10° the increase began at a 1.80 ratio.

The greater-magnitude and lower-temperature drag increases with yaw can be explained in terms of the vortex sheets. As noted in the literature review, increased yaw causes the vortex sheet on the effectively increased sweepback side to move closer to the leading edge root and pivot outwards. This decreases the effect of this vortex sheet on the central area near the trailing edge. On the side

with effectively decreased sweepback, Elle showed that vortex breakdown occurs at lower incidences the lower the leading edge sweep, and that it first occurs far downstream of the trailing edge, moving upstream rather quickly with increasing incidence.[4] This would also reduce the vortex effect on the rear central area. The fact that neither yawing moment data nor rolling moment data in the yawed position varied significantly with increasing temperature shows that both effects roughly balanced each other around the pivot point.

V. CONCLUSIONS

Both the unheated and heated analysis demonstrated the extreme dominance of the vortex sheets in determining the aerodynamic and boundary layer characteristics of the delta wing.

The vortex sheet points of origin and structure are not affected significantly by wall temperature ratios up to 2.0.

The only area where two-dimensional heat transfer theory may have application is in the small conical area at the root trailing edge between the vortex sheets. The rest of the flow is not only highly three-dimensional but temperature insensitive.

The conical area is the only area to show the effects of heating. It experiences the turbulent separation from the rear which is predicted in two-dimensional theory with heating.

The turbulent separation in the conical area becomes more widespread with increasing yaw because of the outward movement of the "downwind" vortex sheet and the increased tendency of the "upwind" vortex sheet to break down with incidence.

Temperature effects are only significant in the upper two-thirds of the effective angle of attack range. Lift shows an almost negligible decrease with temperature through all yaw angles. There is no decrease in the stall angle of attack with temperature. Pitching moment shows a small decrease in stability due to the rear separation. Yawing moment and rolling moment are not affected by heating.

The drag of the wing is strongly temperature dependent. The increasing rear separation with temperature causes a wider wake, and

thus increases the net drag force by forming a larger region of suction pressure acting on the central trailing edge of the wing. The drag increases from 8 per cent to 12 per cent at temperature ratio of 1.8 and from 15 per cent to 25 per cent at a ratio of 2.0 in the angle of attack range of 24° to 33° and a 0° yaw angle.

Increasing yaw angles cause drag increases to occur at lower temperatures and increasing magnitudes with respect to the zero yaw condition. At a yaw of +6° and same angle of attack range, drag increases from 10 per cent to 15 per cent at a temperature ratio of 1.8 and from 18 per cent to 25 per cent at a ratio of 2.0. By a yaw of +10° and same angle of attack range, drag increases from 25 per cent to 35 per cent at a ratio of 1.8 and from 40 per cent to 48 per cent at a ratio of 2.0.

Further research should be undertaken to experimentally test means of reducing the turbulent separation in the conical region. This research would fall naturally into two areas. First, the use of conventional boundary layer control devices such as suction in the conical region to counteract the adverse temperature effects. Secondly, the use of active cooling devices in the conical region to reduce the temperature effects. The feasibility of application of both research areas to vehicles such as the space shuttle would be enhanced by the need to augment only a small region of the total wing surface and the brief time the augmentation would be used.

REFERENCES

1. Macha, J. M. and Norton, D. J., "The Effects of Heat Transfer on the Aerodynamic Characteristics of a Hot Wing," Texas Engineering Experiment Station, Texas A&M University, TEES-1178-TR-72-01, January 1972.

2. Sutton, E. P., "Some Observations of the Flow Over a Delta-Winged Model with 55-Degree Leading-Edge Sweep, at Mach Numbers Between 0.4 and 1.8," A.R.C. Reports and Memoranda No. 3190, November 1955.

3. Garner, H. C. and Bryer, D. W., "Experimental Study of Surface Flow and Part-Span Vortex Layers on a Cropped Arrowhead Wing," A.R.C. Reports and Memoranda No. 3107, November 1955.

4. Elle, B. J., "An Investigation at Low Speed of the Flow Near the Apex of Thin Delta Wings with Sharp Leading Edges," A.R.C. Reports and Memoranda No. 3176, January 1958.

5. Earnshaw, P. B. and Lawford, J. A., "Low-Speed Wind-Tunnel Experiments on a Series of Sharp-Edged Delta Wings," A.R.C. Reports and Memoranda No. 3424, March 1964.

6. Van Driest, E. R., "Investigation of Laminar Boundary Layer in Compressible Fluids Using the Crocco Method," NACA TN 2597, 1952.

7. Libby, P. A., Morduchow, M. and Bloom, M., "Critical Study of Integral Methods in Compressible Laminar Boundary Layers," NACA TN 2655, 1952.

8. Morduchow, M. and Clarke, J. H., "Method for Calculation of Compressible Laminar Boundary-Layer Characteristics in Axial Pressure Gradient with Zero Heat Transfer," NACA TN 2784, 1952.

9. Bloom, M., "The Effect of Surface Cooling on Laminar Boundary Layer Stability," JAS, September 1951, pp. 635-636.

10. Libby, P. A. and Morduchow, M., "Method for Calculation of Compressible Laminar Boundary Layer with Axial Pressure Gradient and Heat Transfer," NACA TN 3157, 1954.

11. Morduchow, M. and Grape, R. G., "Separation, Stability, and Other Properties of Compressible Laminar Boundary Layer with Pressure Gradient and Heat Transfer," NACA TN 3296, 1955.

12. Morduchow, M., "Analysis and Calculation by Integral Methods of Laminar Compressible Boundary Layer with Heat Transfer and With and Without Pressure Gradient," NACA Report 1245, 1955.

13. Walz, A., Boundary Layers of Flow and Temperature, edited and translated by Hans Joerg Oser, M.I.T. Press, Cambridge, Massachusetts, 1969.

14. Cebeci, T., Smith, A.M.O. and Wang, L.C., "A Finite-Difference Method for Calculating Compressible Laminar and Turbulent Boundary Layers," Parts I and II, Report No. DAC-67131, McDonnell Douglas Aircraft Company, Inc., March 1969.

15. Mironer, A., "Accelerated Diffusion of Wing Tip Vortices by Heating," AIAA Paper No. 71-616, June 1971.

16. Costen, R. C., "Drift of Buoyant Wing-Tip Vortices," JA, p. 406, 1972.

17. Haines, A.B., "Some Notes on the Flow Patterns Observed Over Various Swept-back Wings at Low Mach Numbers," A.R.C. Reports and Memoranda No. 3192, September 1954.

APPENDIX A

ERROR ANALYSIS

The basic experimental errors introduced in each mechanical aspect of the research are as follows:

1. Freestream temperature varied in two ways during the tests. The maximum variation of the freestream temperature from the average of all runs was $\pm$ 16°F. The instantaneous temperature varied from the average for each run by a maximum of $\pm$ 12°F.
2. Flow angularity error based on calibrations by previous investigators was $\pm$ 0.3° in pitch and $\pm$ 0.3° in yaw.
3. Tunnel dynamic pressure varied an estimated maximum of $\pm$ 2% during the tests.
4. Angle of attack error at each station was a maximum of $\pm$ 0.017°. Angle of sideslip error at each station was a maximum of $\pm$ 0.015°.
5. Surface temperature varied in two ways during the tests. The maximum variation from the indication given by the average-temperature thermocouple was $\pm$ 60°F at the starts of the runs and $\pm$ 15°F at the ends of the runs across the surface of the wing. The instantaneous error of the average-temperature thermocouple was estimated to be a maximum of $\pm$ 5°F.

The errors in the calculations of the coefficients were analyzed using the square root of the sum of the squares method. Two of the equations are shown and the rest are similar.

$$\Delta C_L = \sqrt{\left(\frac{\partial C_L}{\partial q}\Delta q\right)^2 + \left(\frac{\partial C_L}{\partial S}\Delta S\right)^2 + \left(\frac{\partial C_L}{\partial L}\Delta L\right)^2}$$

$$\Delta C_M = \sqrt{\left(\frac{\partial C_M}{\partial q}\Delta q\right)^2 + \left(\frac{\partial C_M}{\partial S}\Delta S\right)^2 + \left(\frac{\partial C_M}{\partial \bar{c}}\Delta \bar{c}\right)^2 + \left(\frac{\partial C_M}{\partial M}\Delta M\right)^2}$$

The span instead of the chord is used for rolling and yawing moments. The wing span and mean aerodynamic chord errors are estimated as 0.5 per cent. Force and moment errors (ΔL or ΔM) were obtained by averaging twenty data points in a run under equilibrium conditions and taking the maximum derivation from that average. The results are shown in Table 3 for $\beta = 0°$.

TABLES

TABLE 1

WING CHARACTERISTICS

Airfoil section	Modified double wedge
Leading-edge radius, per cent chord	0.791
Leading-edge sweep angle, deg	60
Wing thickness, per cent chord	8
Dihedral angle, deg	0
Twist, deg	0
Area, sq. in.	576
Span, in.	36.5
Mean aerodynamic chord, in.	21.1
Aspect ratio	2.31

TABLE 2

MATERIAL CHARACTERISTICS

Material	Aluminum alloy 356
Density, lb/ft^3	0.097
Melting point, °F	1035 +
Thermal conductivity, $Btu/hr/ft^2$	92
Coefficient of thermal expansion, $°F^{-1}$	11.9×10^{-6}
Tensile strength, ksi	25
Yield strength, ksi	20
Elongation (2 in.), per cent	2.0

TABLE 3

ERROR ANALYSIS

Error	$\alpha = 26°$	$\alpha = 32°$
ΔC_L	0.0130	0.0132
ΔC_D	0.0021	0.0031
ΔC_Y	0.0010	0.0020
ΔC_M	0.0027	0.0030
ΔC_n	0.0002	0.0004
ΔC_ℓ	0.0002	0.0004

FIGURES

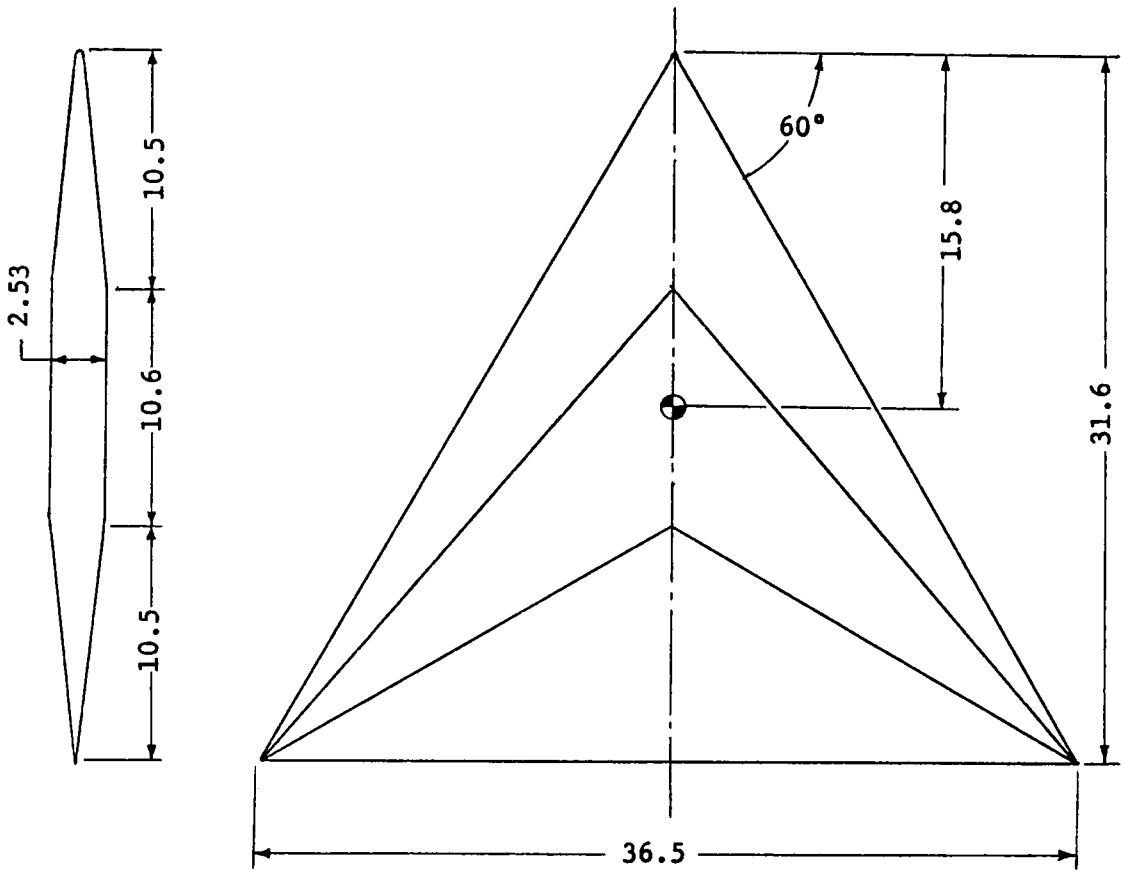

Figure 1. Sketch of model used in tests. All dimensions in inches.

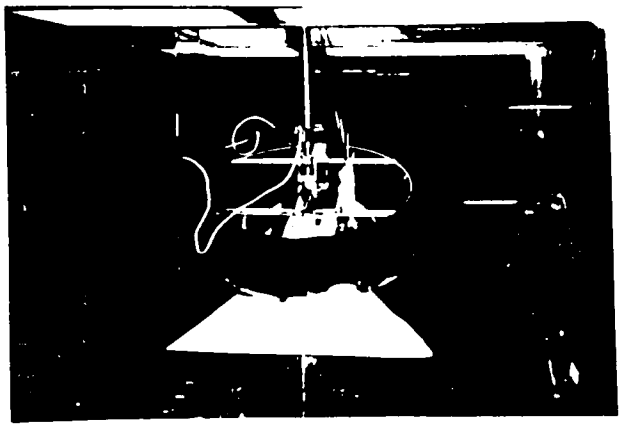

Fig. 2 Delta wing installed in tunnel, heater partially retracted.

Fig. 3 Delta wing with heater lowered to operating position.

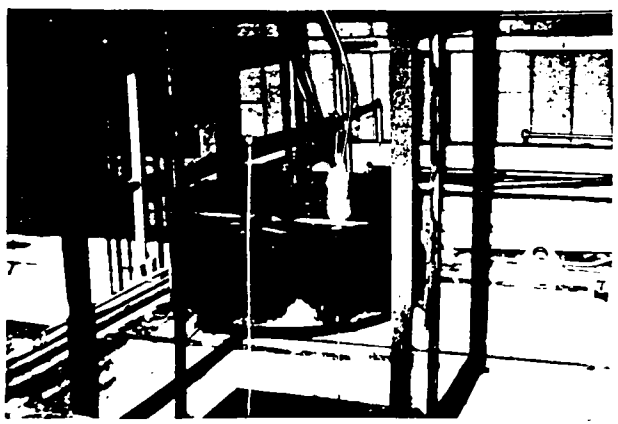

Fig. 4 Heater retracted to position to top of wind tunnel.

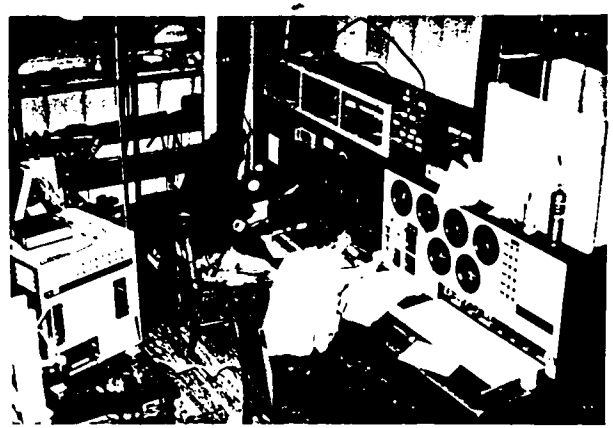

Fig. 5 Test instrumentation with tunnel controls, readout, and temperature monitors.

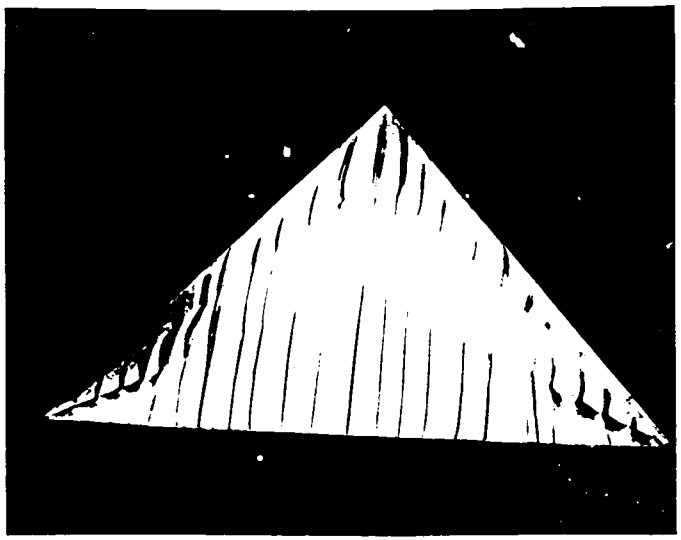

Fig. 6 Oil flow patterns, $\alpha = 0^{o}$, $\beta = 0^{o}$.

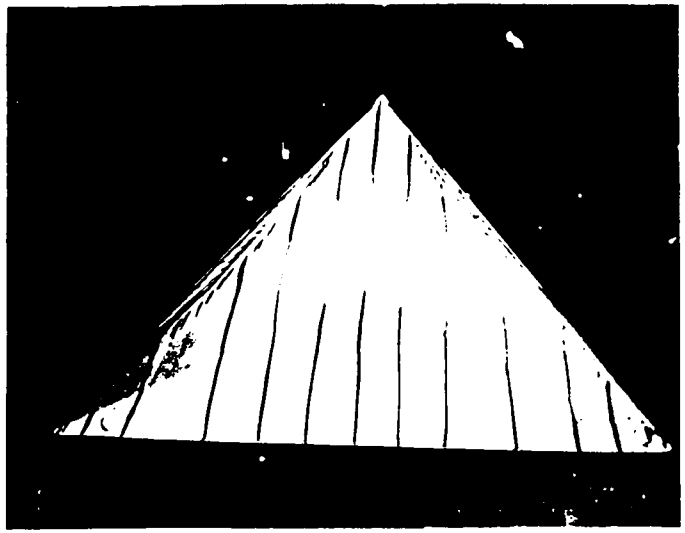

Fig. 7 Oil flow patterns, $\alpha = 4^{o}$, $\beta = 0^{o}$.

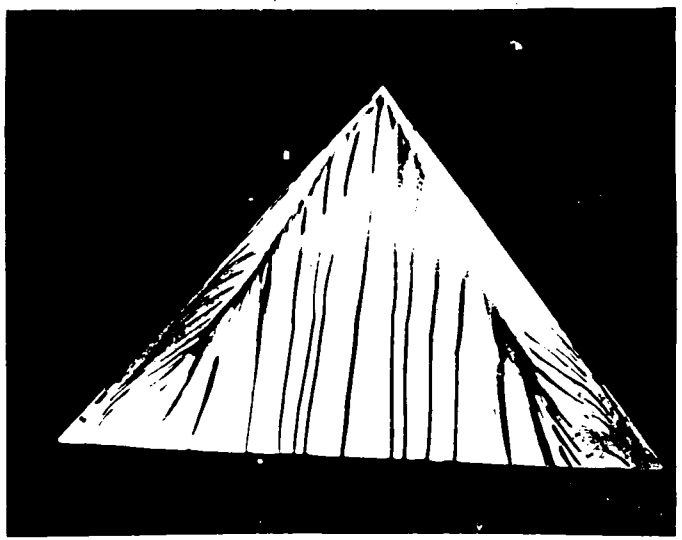

Fig. 8 Oil flow patterns, $\alpha = 8^{o}$, $\beta = 0^{o}$.

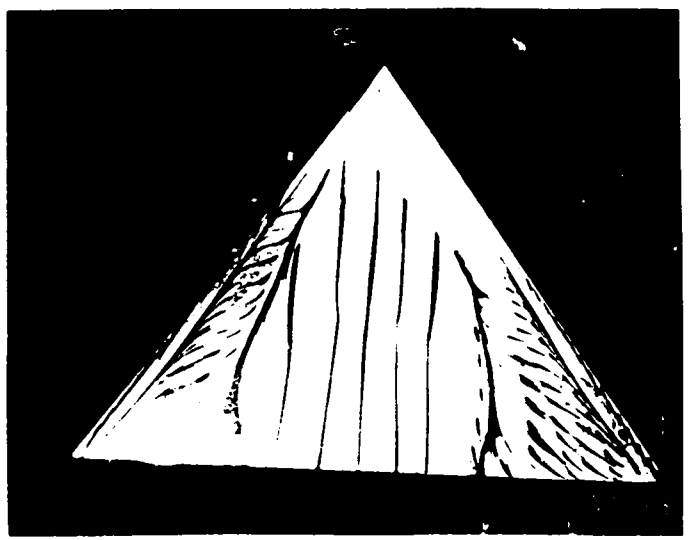

Fig. 9 Oil flow patterns, $\alpha = 16^{o}$, $\beta = 0^{o}$.

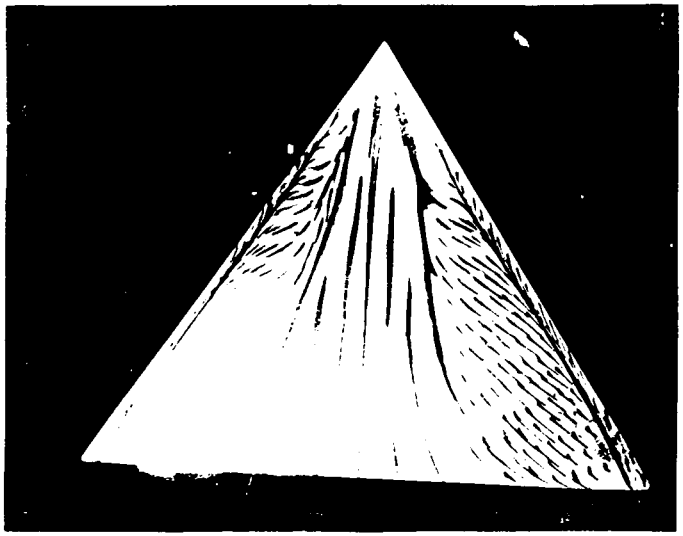

Fig. 10 Oil flow patterns, $\alpha = 24^{o}$, $\beta = 0^{o}$.

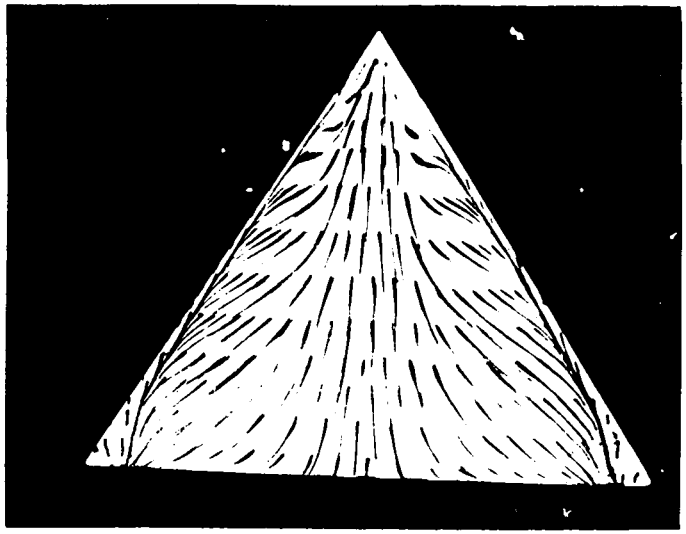

Fig. 11 Oil flow patterns, $\alpha = 28^{o}$, $\beta = 0^{o}$.

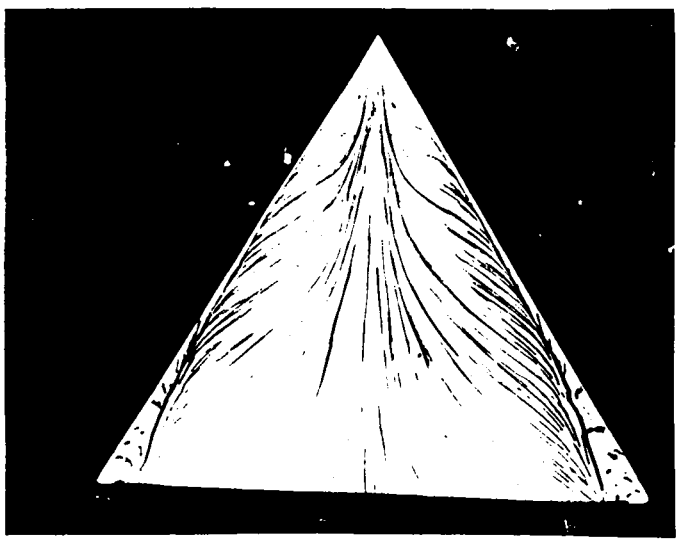

Fig. 12 Oil flow patterns, $\alpha = 32^{o}$, $\beta = 0^{o}$.

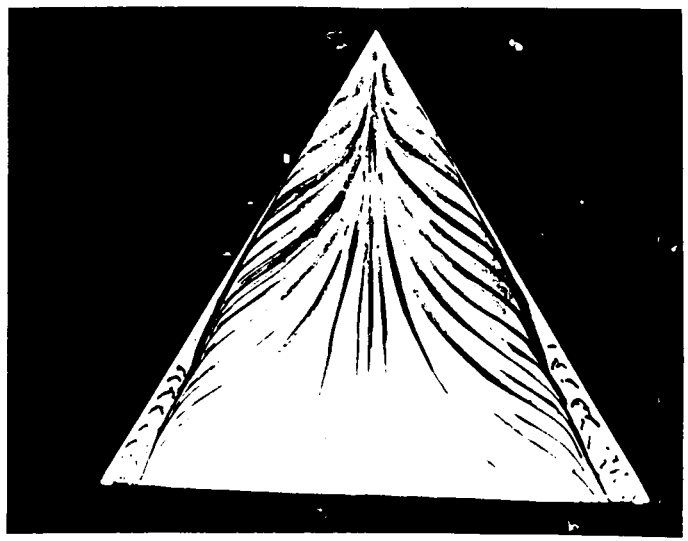

Fig. 13 Oil flow patterns, $\alpha = 36^{o}$, $\beta = 0^{o}$.

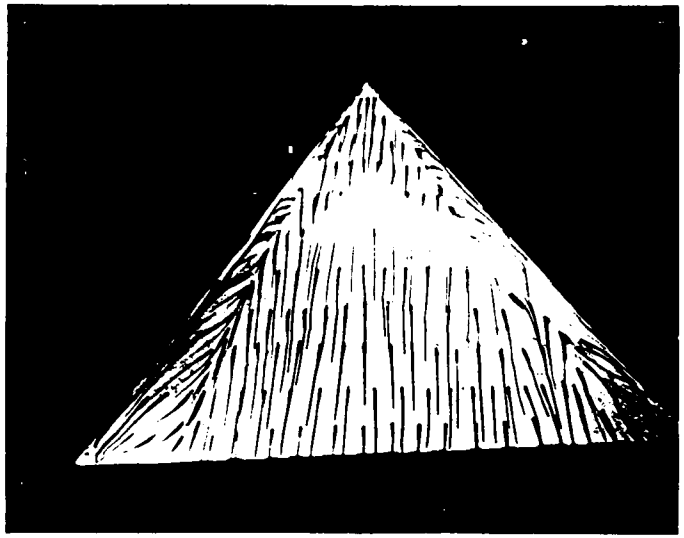

Fig. 14 Oil flow patterns, $\alpha = 8^{o}$, $\beta = 6^{o}$.

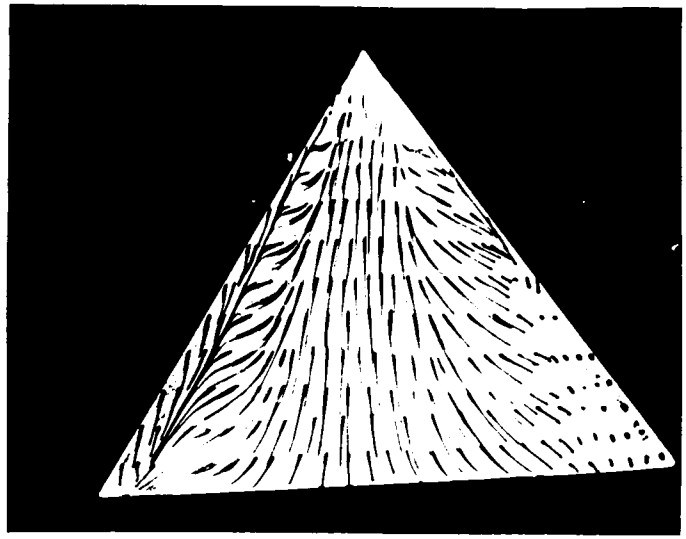

Fig. 15 Oil flow patterns, $\alpha = 24^{o}$, $\beta = 6^{o}$.

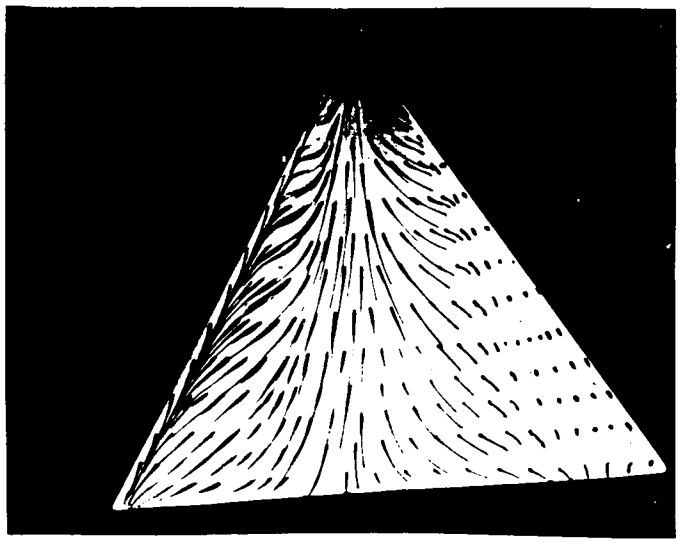

Fig. 16 Oil flow patterns, $\alpha = 32^{o}$, $\beta = 6^{o}$.

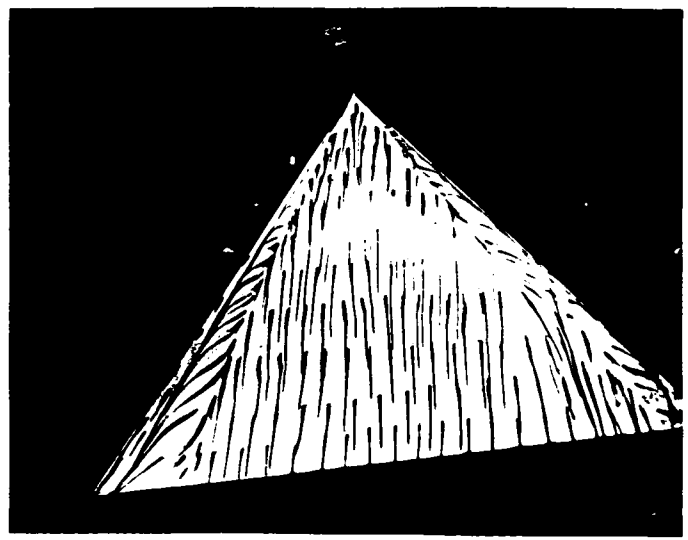

Fig. 17 Oil flow patterns, $\alpha = 8^{o}$, $\beta = 10^{o}$.

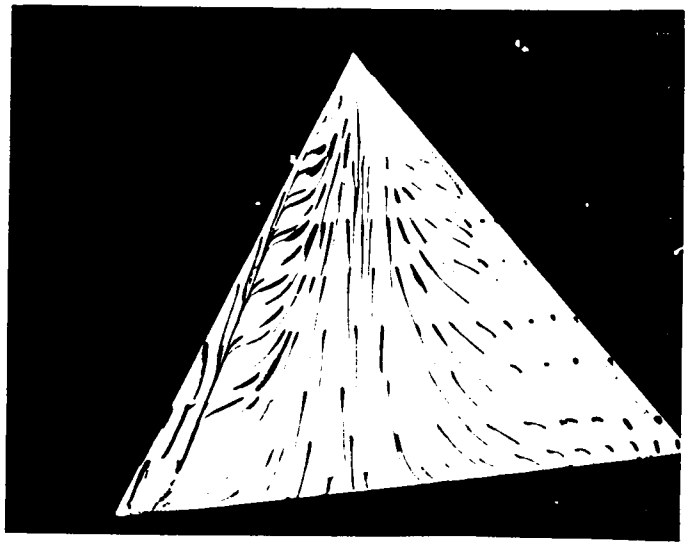

Fig. 18 Oil flow patterns, $\alpha = 24^{o}$, $\beta = 10^{o}$.

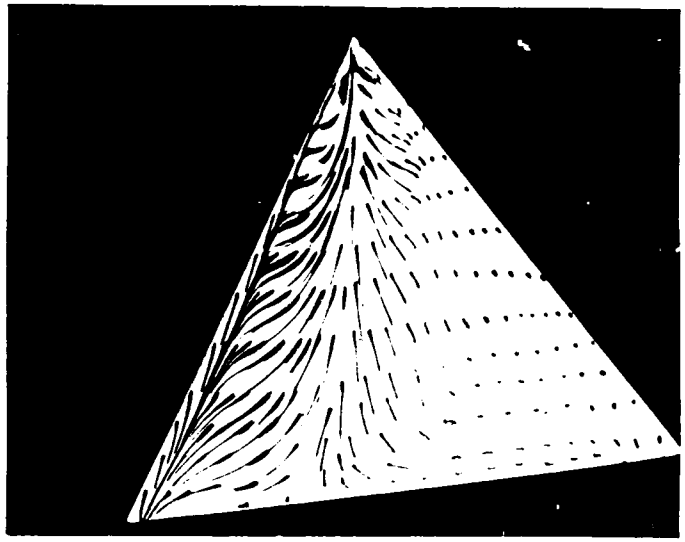

Fig. 19 Oil flow patterns, $\alpha = 32^{o}$, $\beta = 10^{o}$.

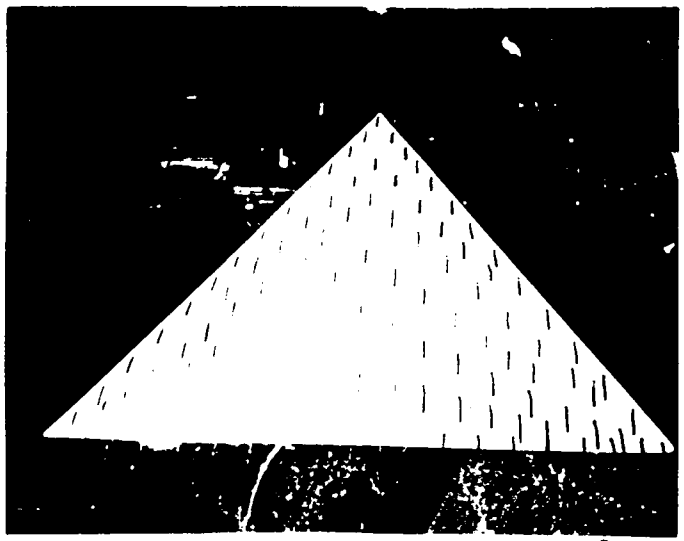

Fig. 20 Tuft patterns, $\alpha = 0^{o}$, $\beta = 0^{o}$.

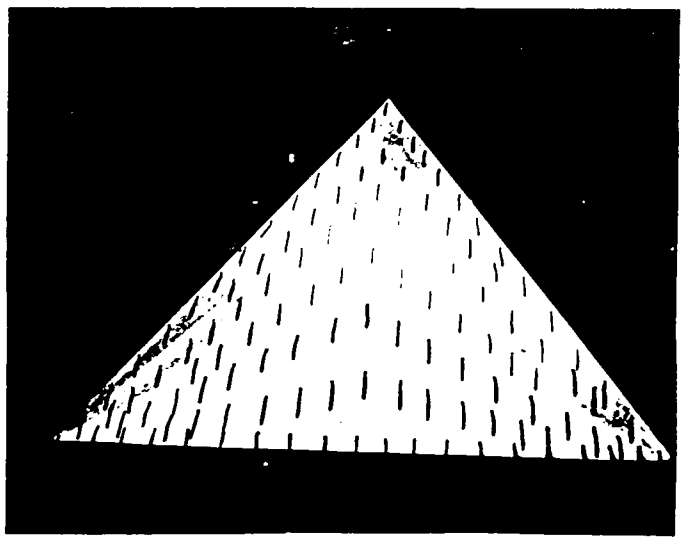

Fig. 21 Tuft patterns, $\alpha = 4^{o}$, $\beta = 0^{o}$.

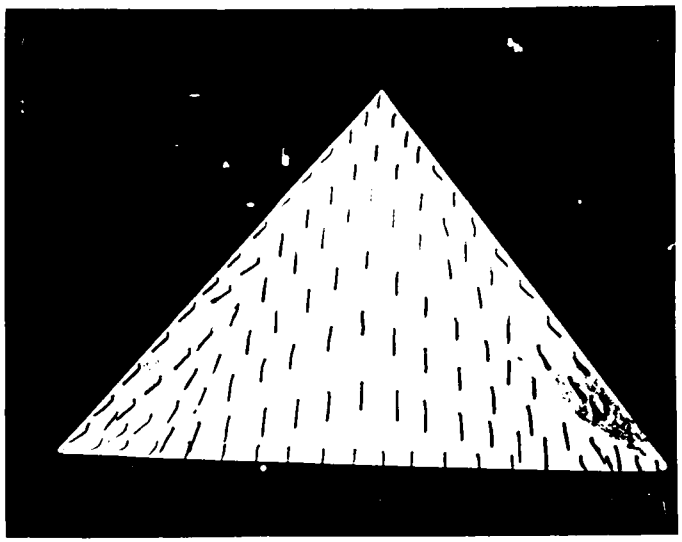

Fig. 22 Tuft patterns, $\alpha = 8^{o}$, $\beta = 0^{o}$.

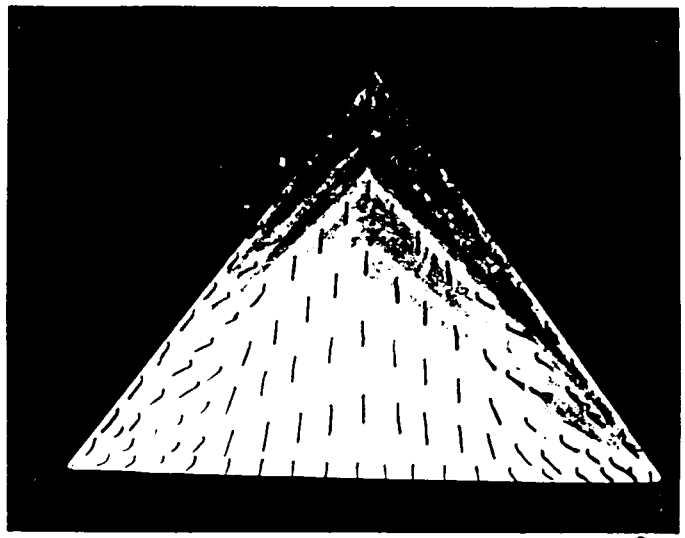

Fig. 23 Tuft patterns, $\alpha = 16^{o}$, $\beta = 0^{o}$.

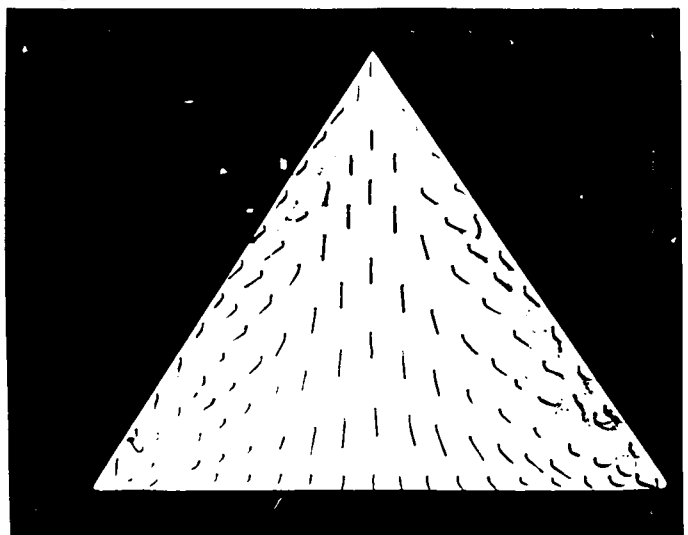

Fig. 24 Tuft patterns, $\alpha = 24^{o}$, $\beta = 0^{o}$.

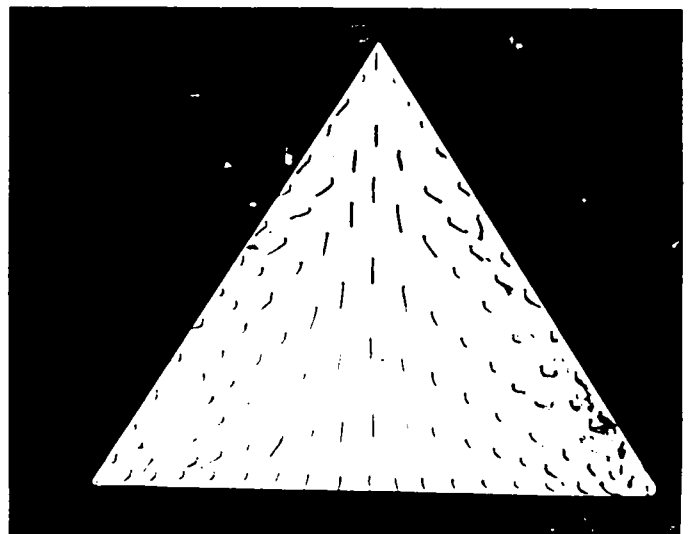

Fig. 25 Tuft patterns, $\alpha = 28^{o}$, $\beta = 0^{o}$.

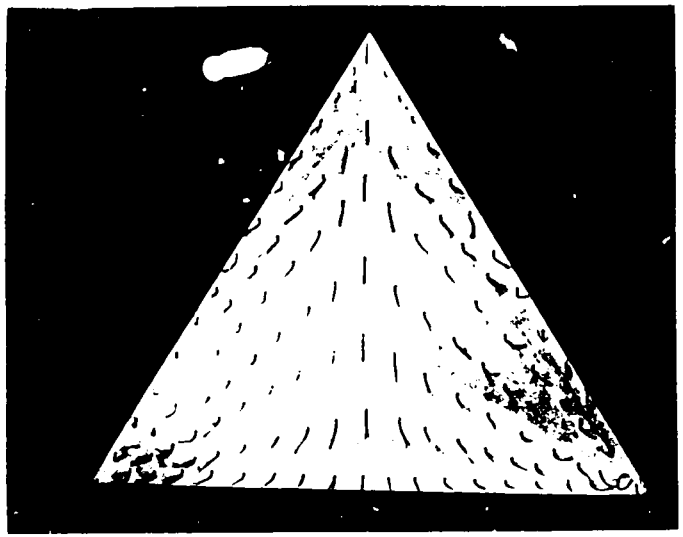

Fig. 26 Tuft patterns, $\alpha = 32^{o}$, $\beta = 0^{o}$.

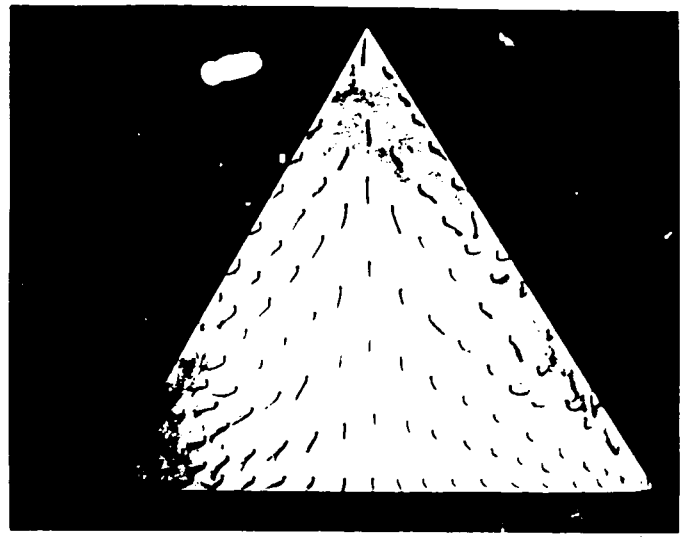

Fig. 27 Tuft patterns, $\alpha = 36^{o}$, $\beta = 0^{o}$.

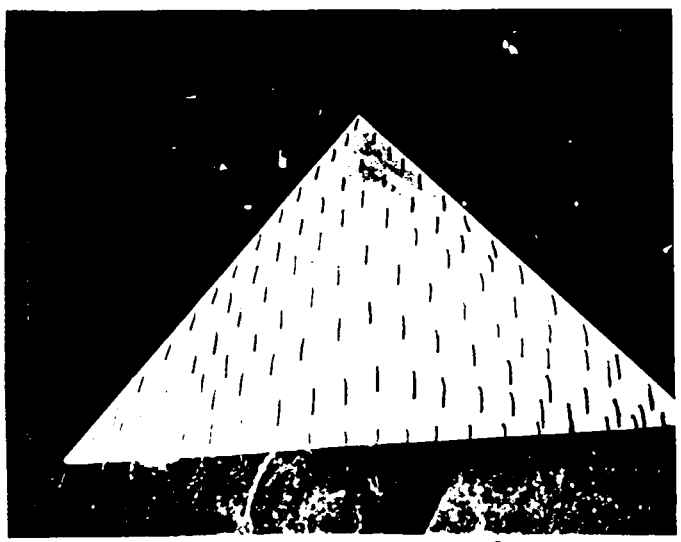

Fig. 28 Tuft patterns, $\alpha = 0^{o}$, $\beta = 6^{o}$.

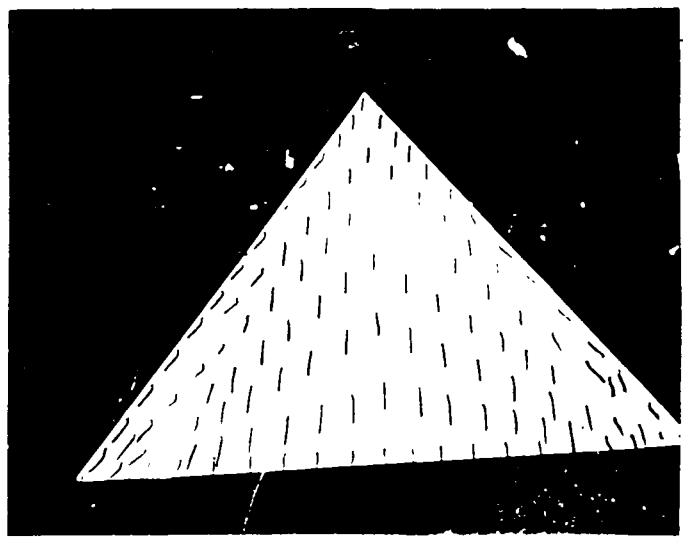

Fig. 29 Tuft patterns, $\alpha = 8^{o}$, $\beta = 6^{o}$.

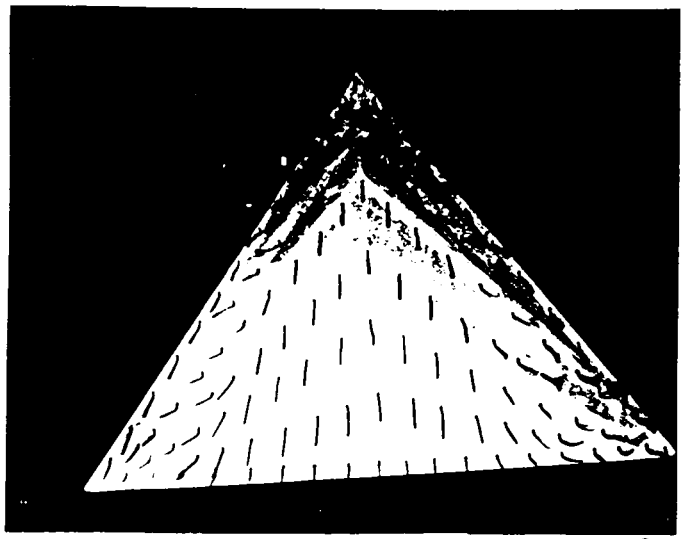

Fig. 30 Tuft patterns, $\alpha = 16^{o}$, $\beta = 6^{o}$.

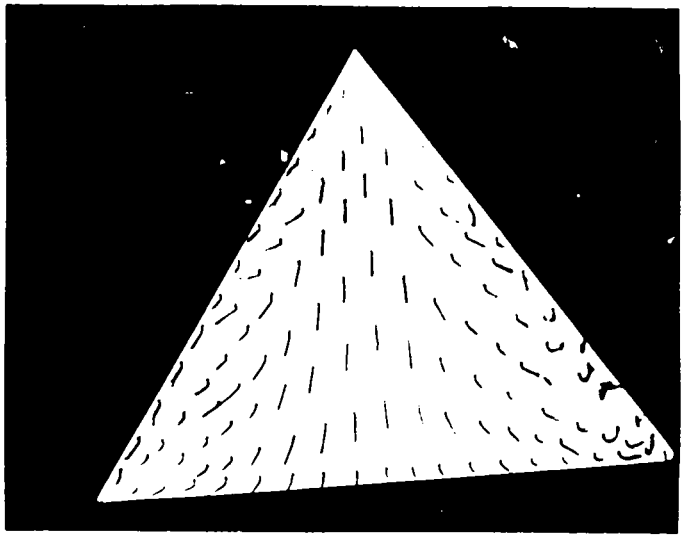

Fig. 31 Tuft patterns, $\alpha = 24^{o}$, $\beta = 6^{o}$.

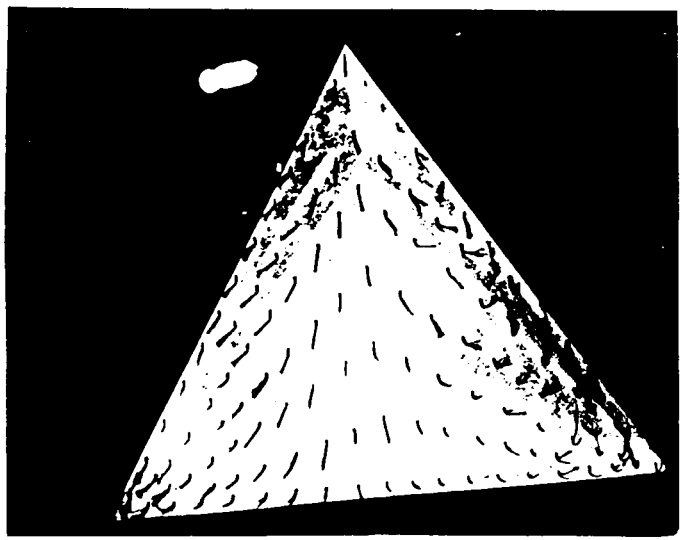

Fig. 32 Tuft patterns, $\alpha = 32^{o}$, $\beta = 6^{o}$.

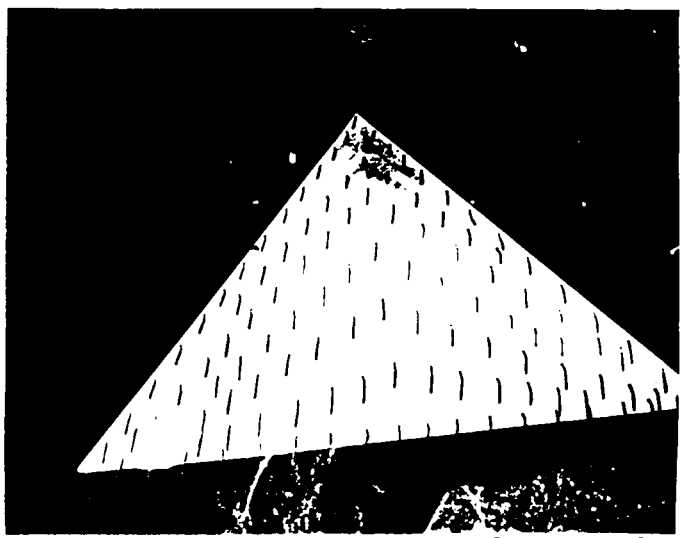

Fig. 33 Tuft patterns, $\alpha = 0^{o}$, $\beta = 10^{o}$.

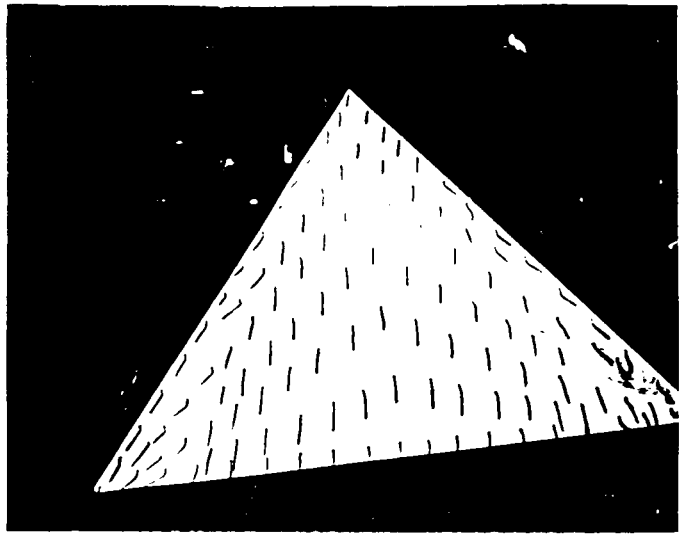

Fig. 34 Tuft patterns, $\alpha = 8^{o}$, $\beta = 10^{o}$.

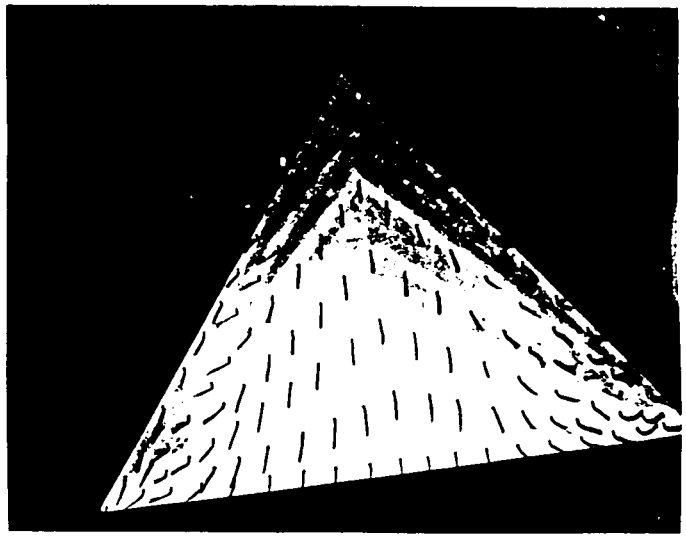

Fig. 35 Tuft patterns, $\alpha = 16^{o}$, $\beta = 10^{o}$.

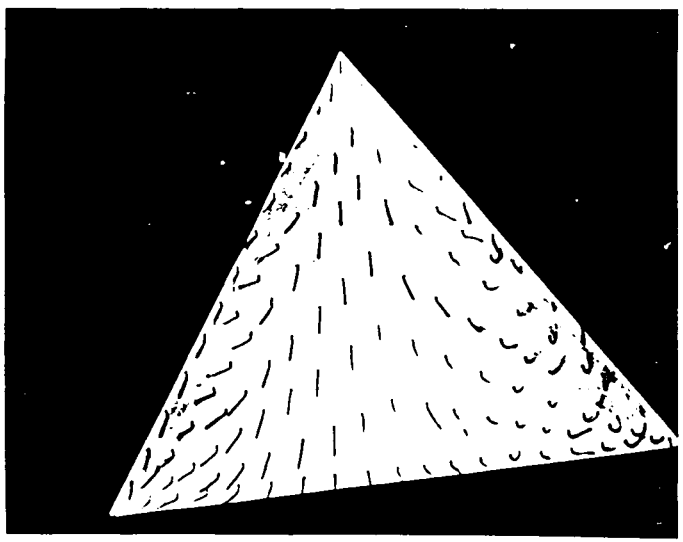

Fig. 36 Tuft patterns, $\alpha = 24^{o}$, $\beta = 10^{o}$.

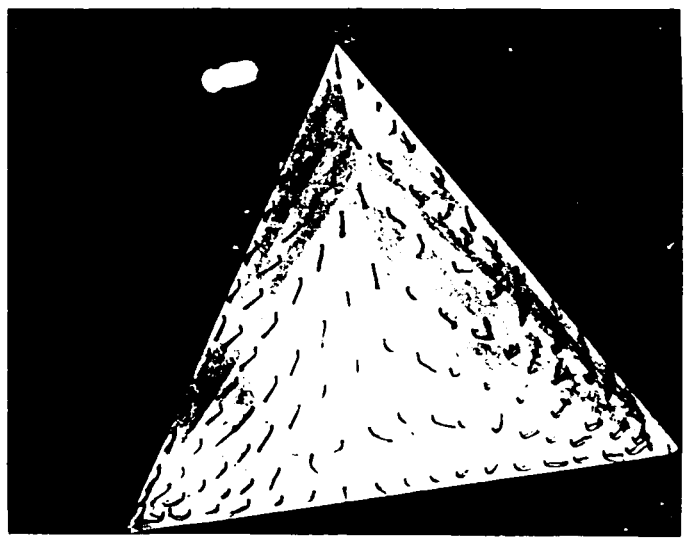

Fig. 37 Tuft patterns, $\alpha = 32^{o}$, $\beta = 10^{o}$.

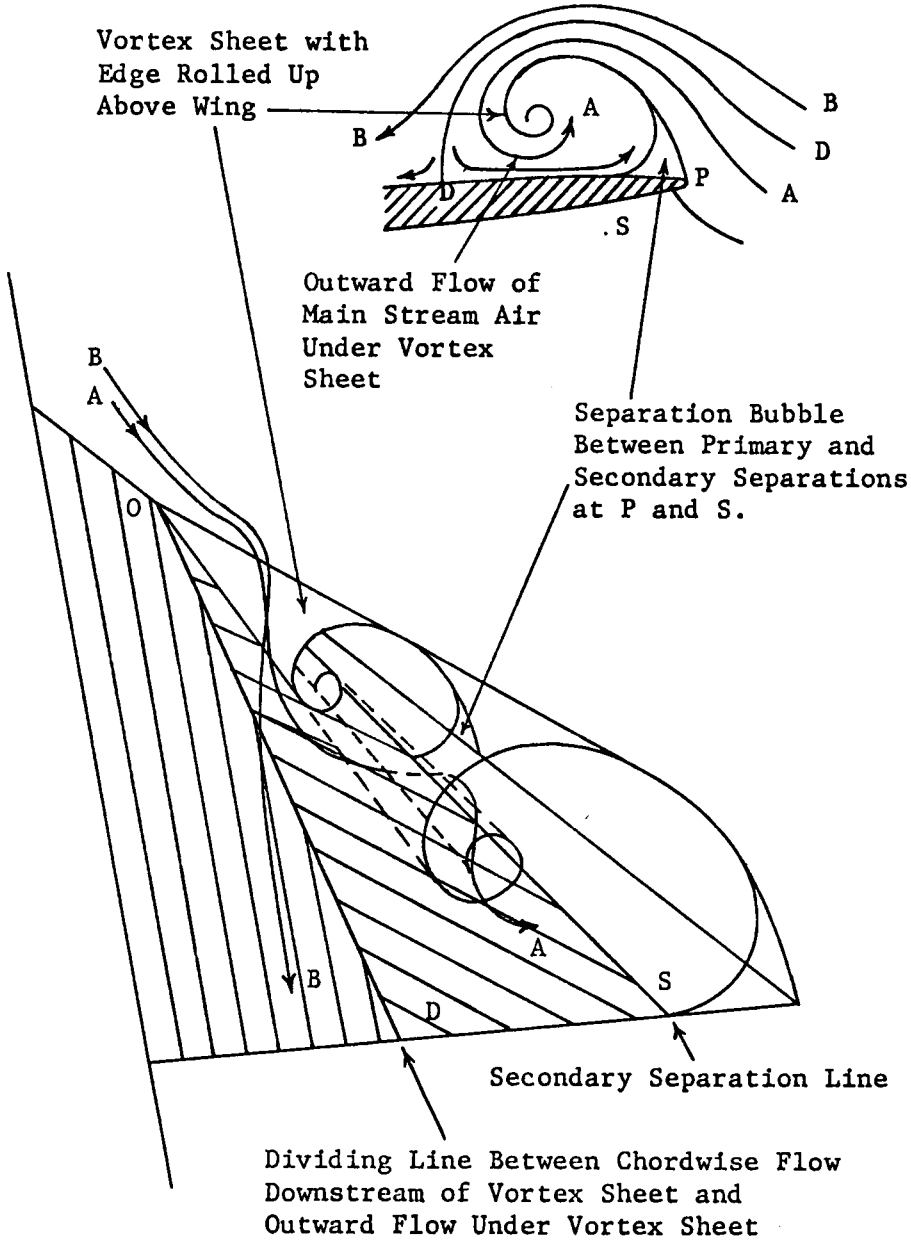

Figure 38. Sketch of main features of flow with leading-edge separation and vortex sheet.

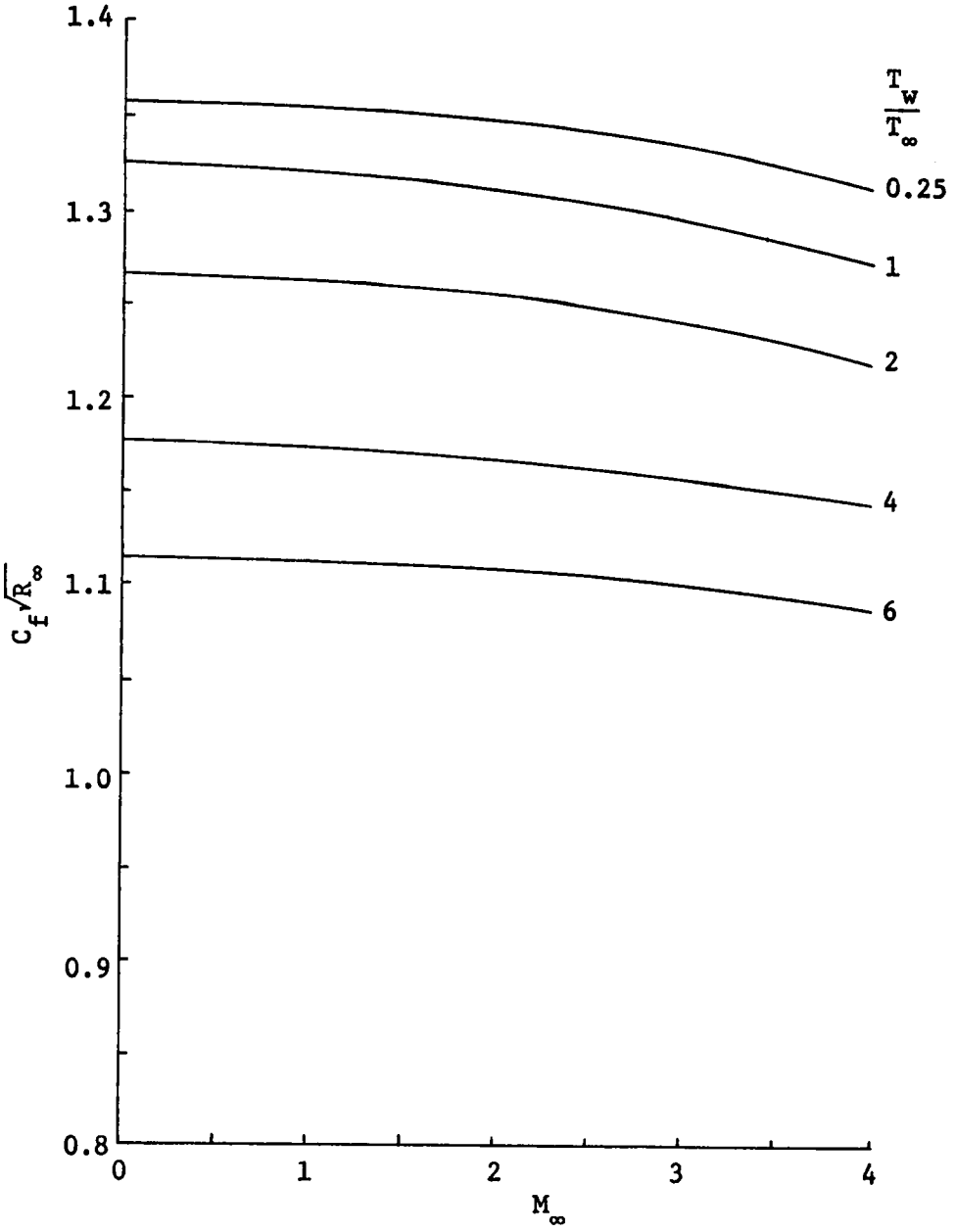

Figure 39. Mean Skin-friction Coefficient for Laminar Boundary Layer of a Compressible Fluid Flowing Along a Flat Plate.

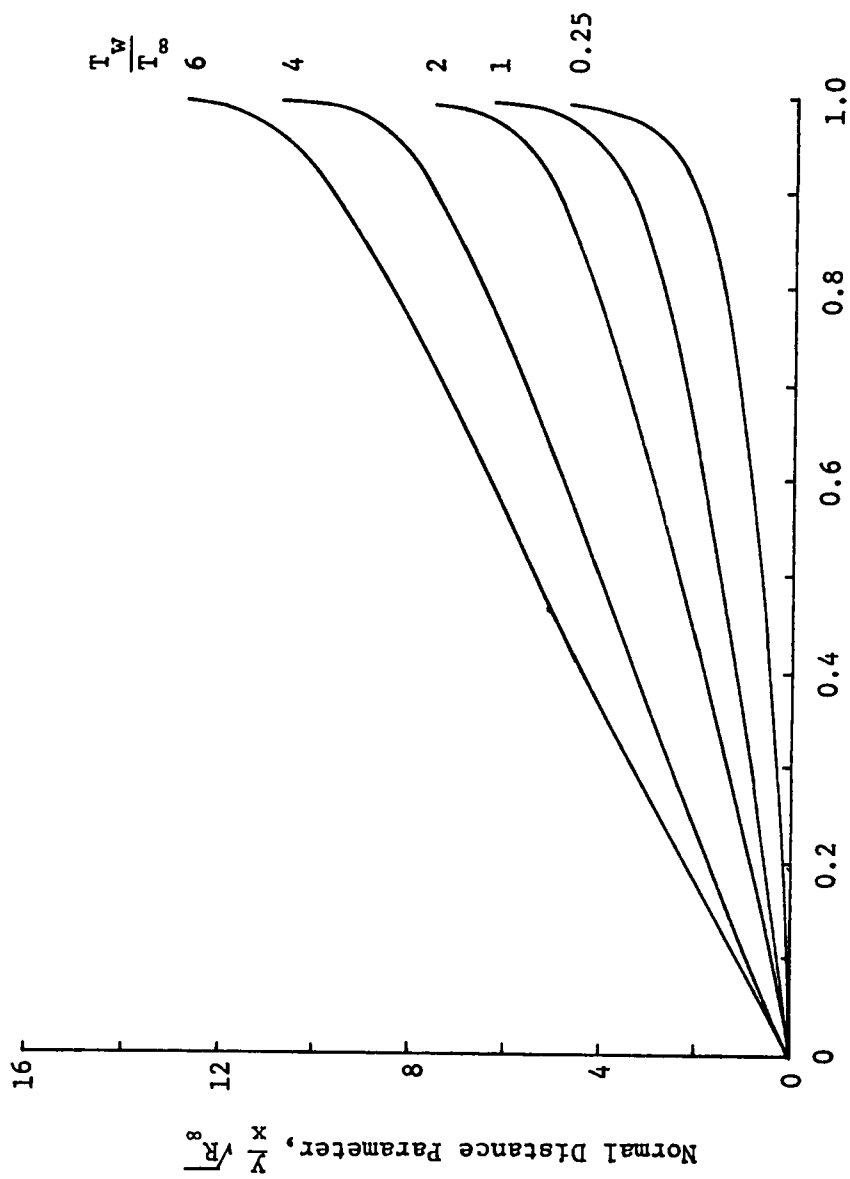

Figure 40. Velocity Distribution Across Laminar Boundary Layer for $M_\infty = 0$ and Various T_w/T_∞.

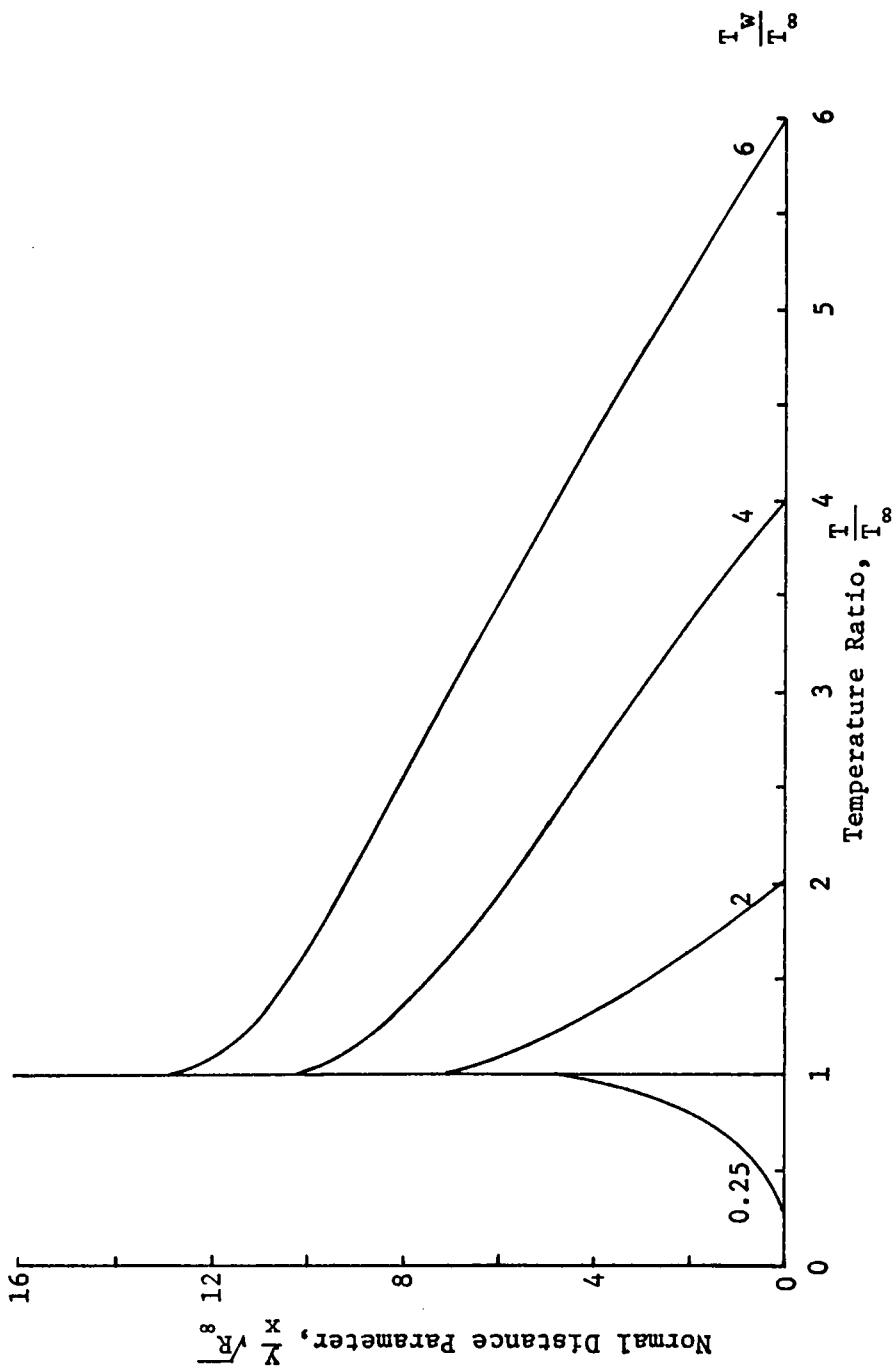

Figure 41. Temperature Distribution Across Laminar Boundary Layer for $M_\infty = 0$ and Various T_w/T_∞

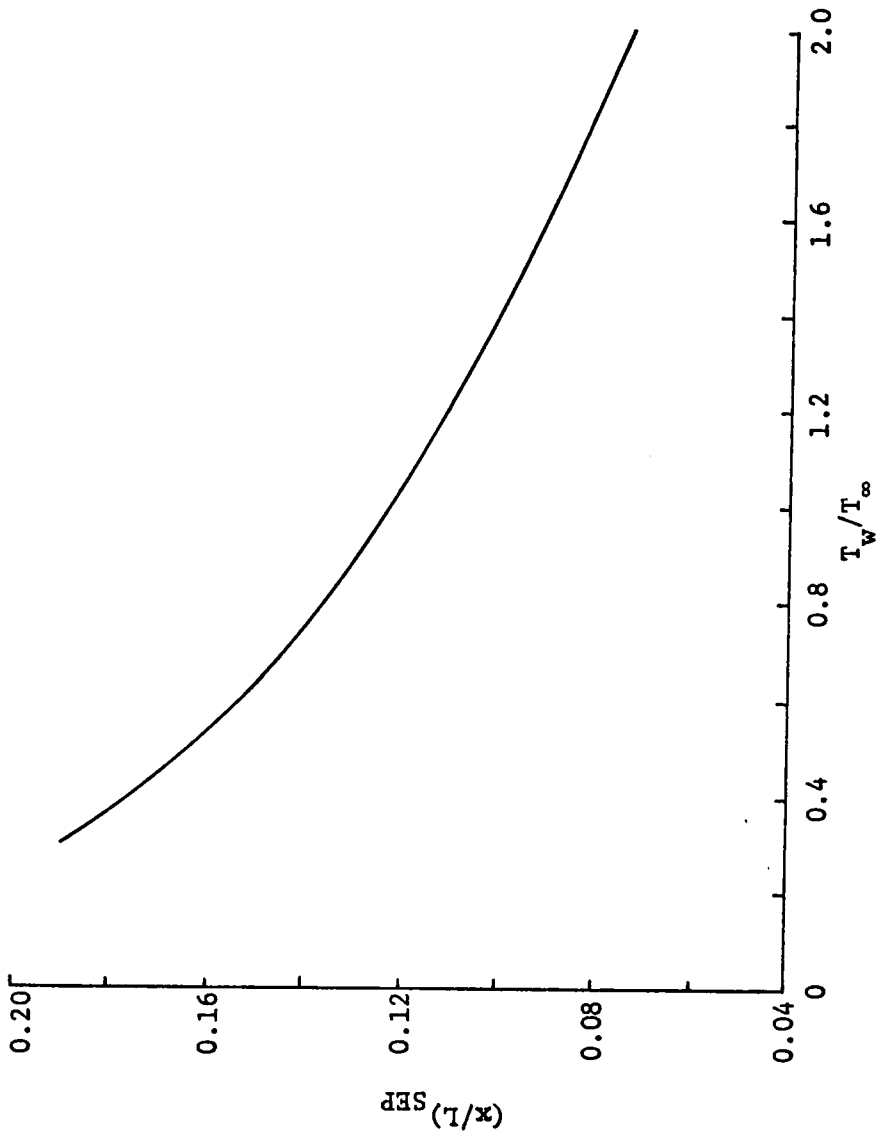

Figure 42. Separation Point as a Function of Wall Temperature for $M_\infty = 0$ and Laminar Flow.

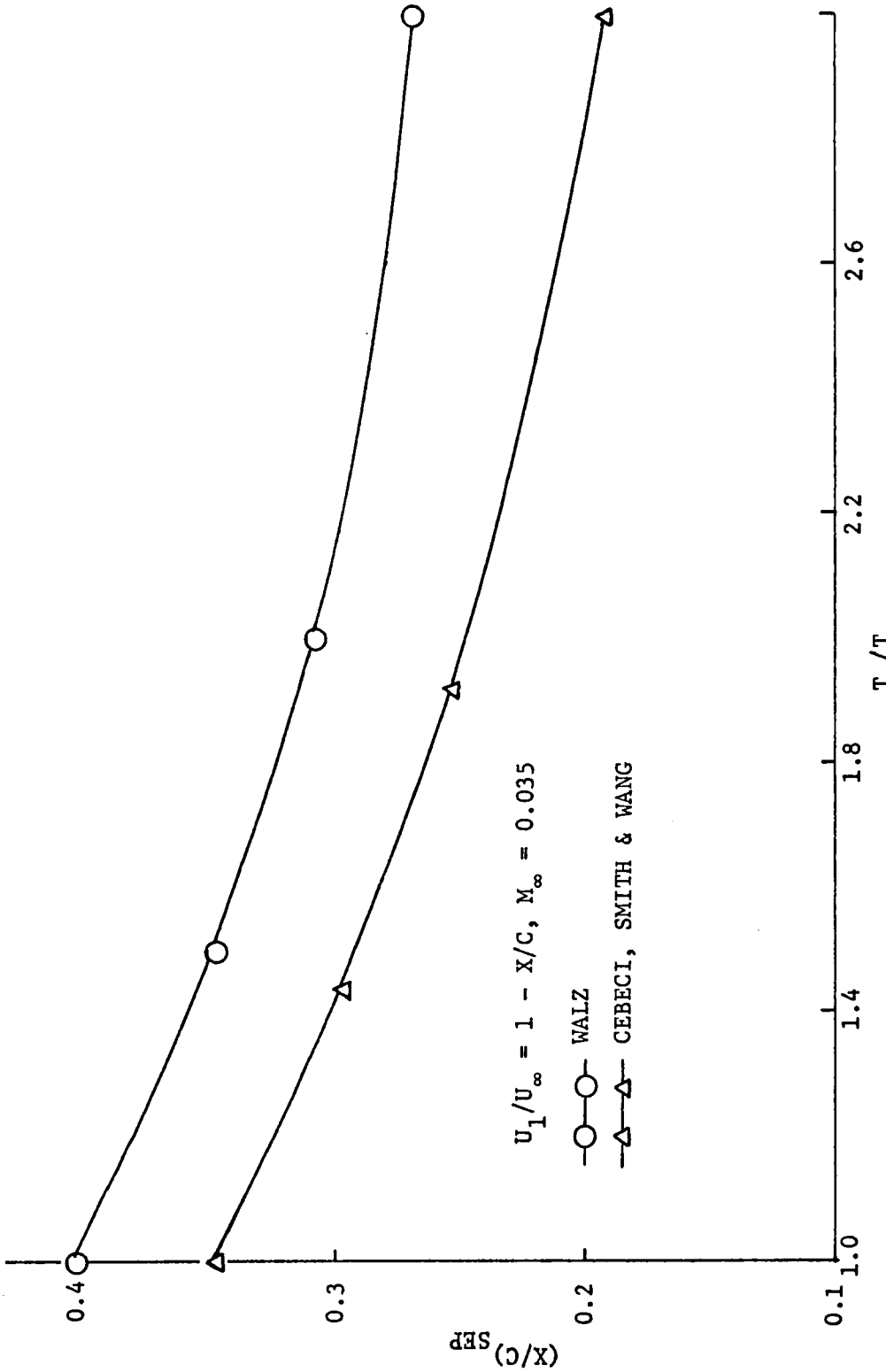

Figure 43.[8] Effect of Surface Temperature on Turbulent Separation.

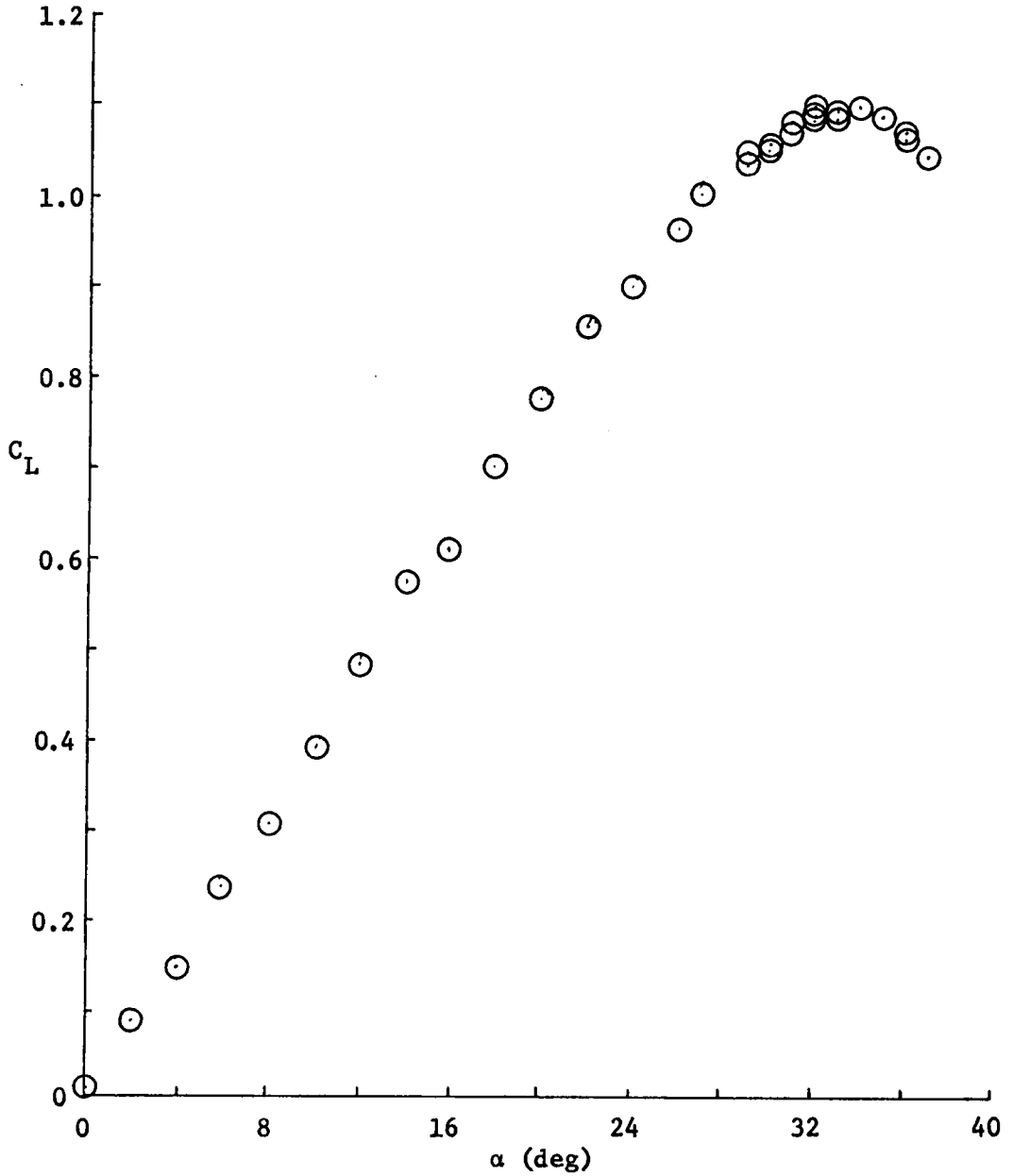

Figure 44. Lift Versus Angle of Attack, $\beta = 0°$.

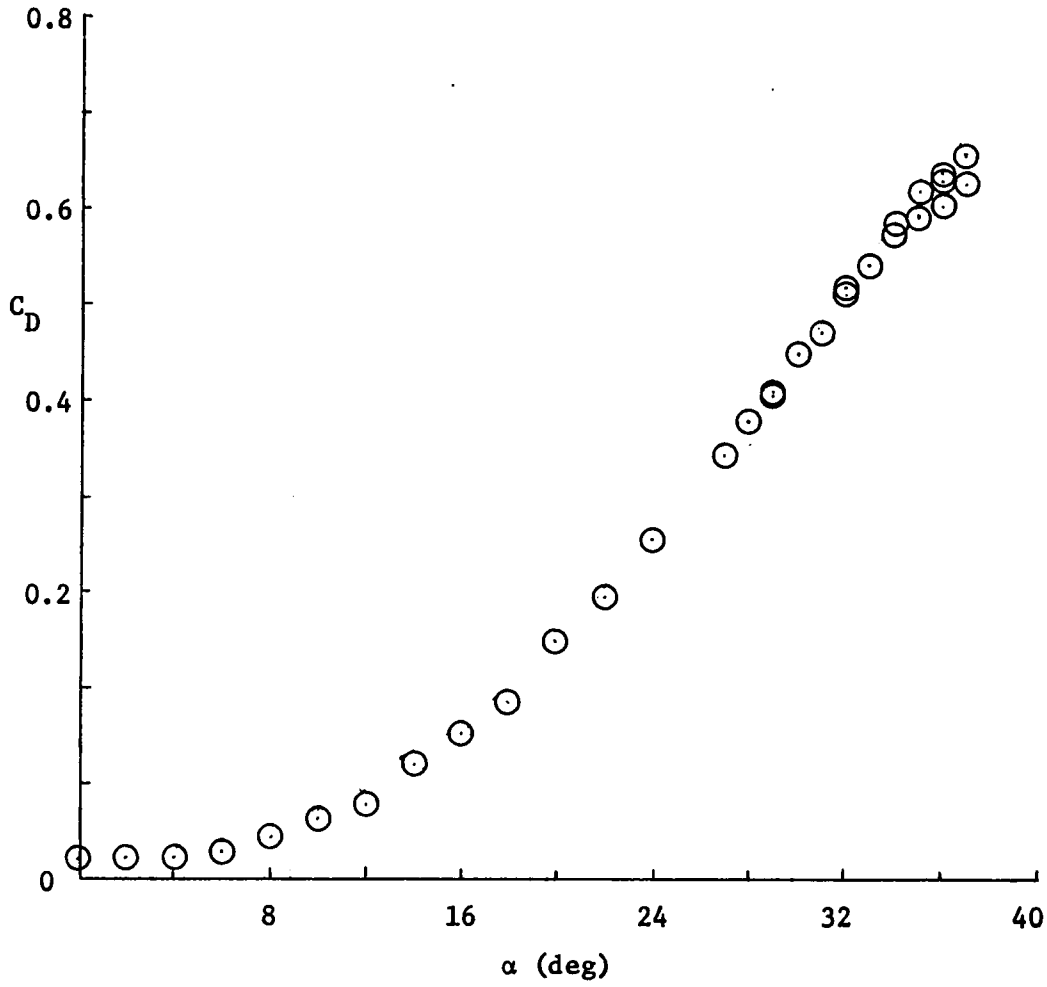

Figure 45. Drag Versus Angle of Attack, $\beta = 0°$.

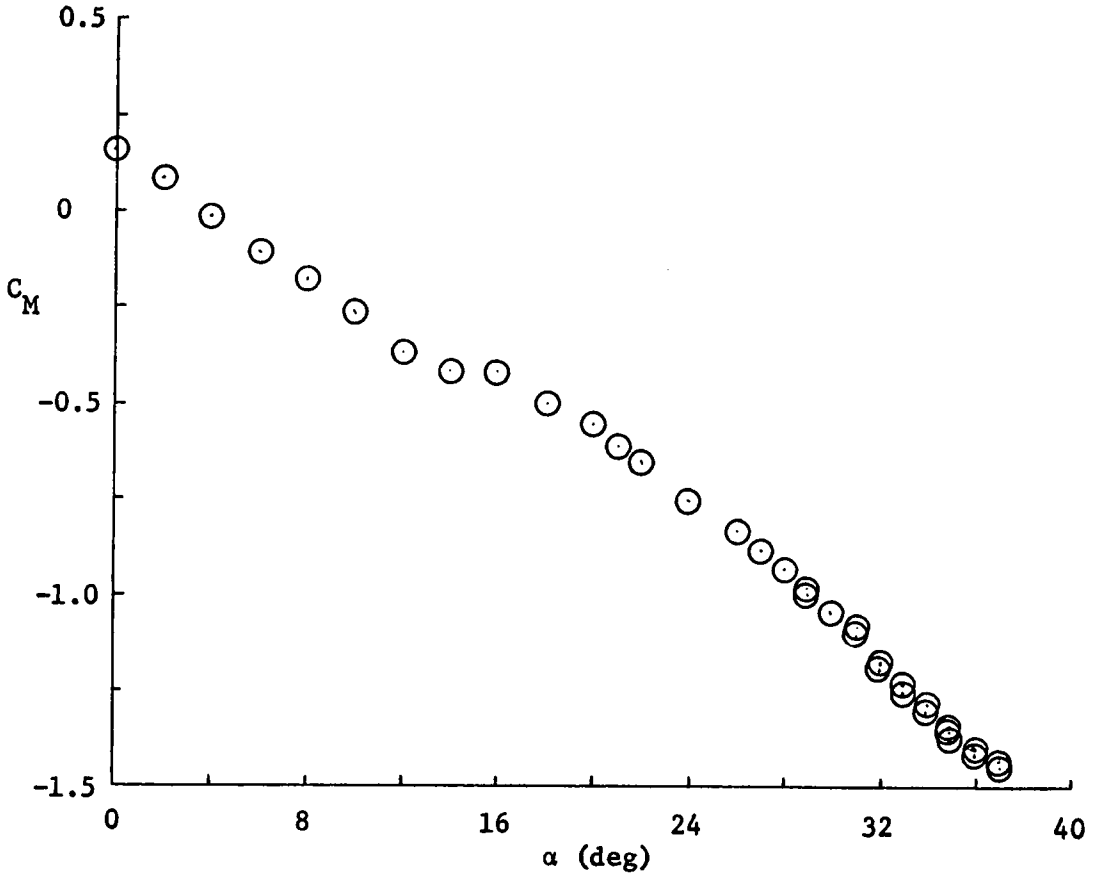

Figure 46. Pitching Moment Versus Angle of Attack, $\beta = 0°$.

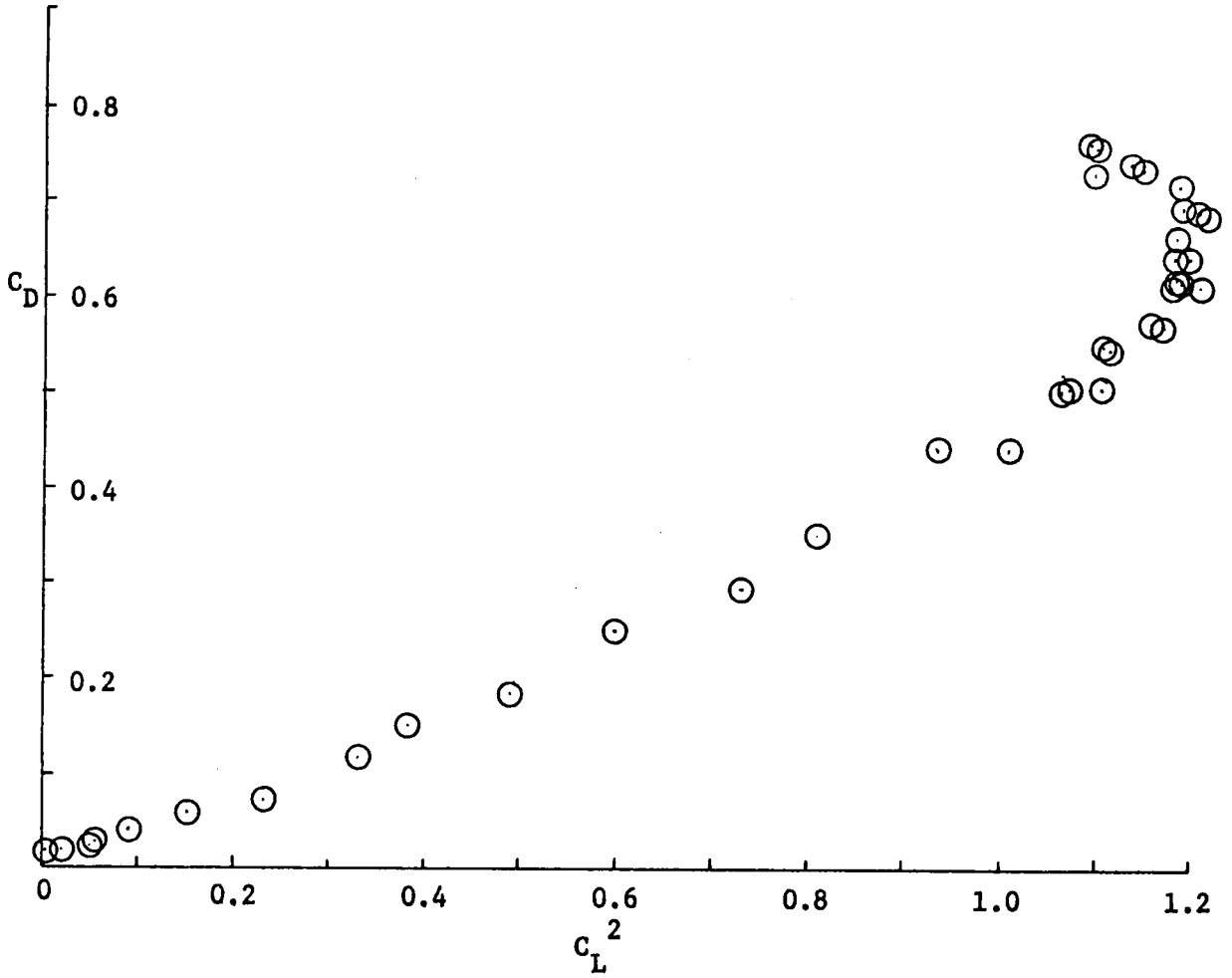

Figure 47. Drag Versus the Square of the Lift, $\beta = 0°$.

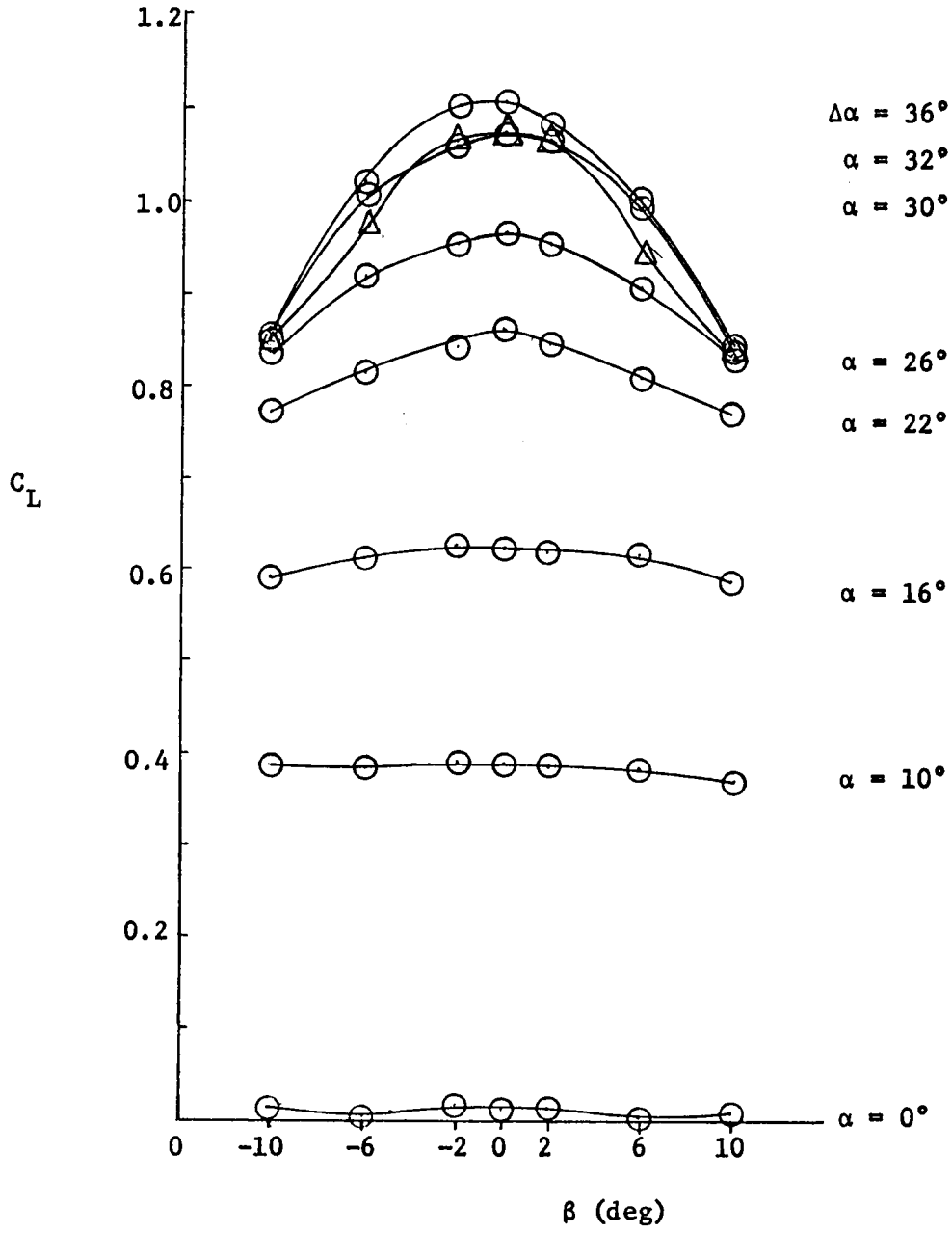

Figure 48. Lift Versus Angle of Yaw.

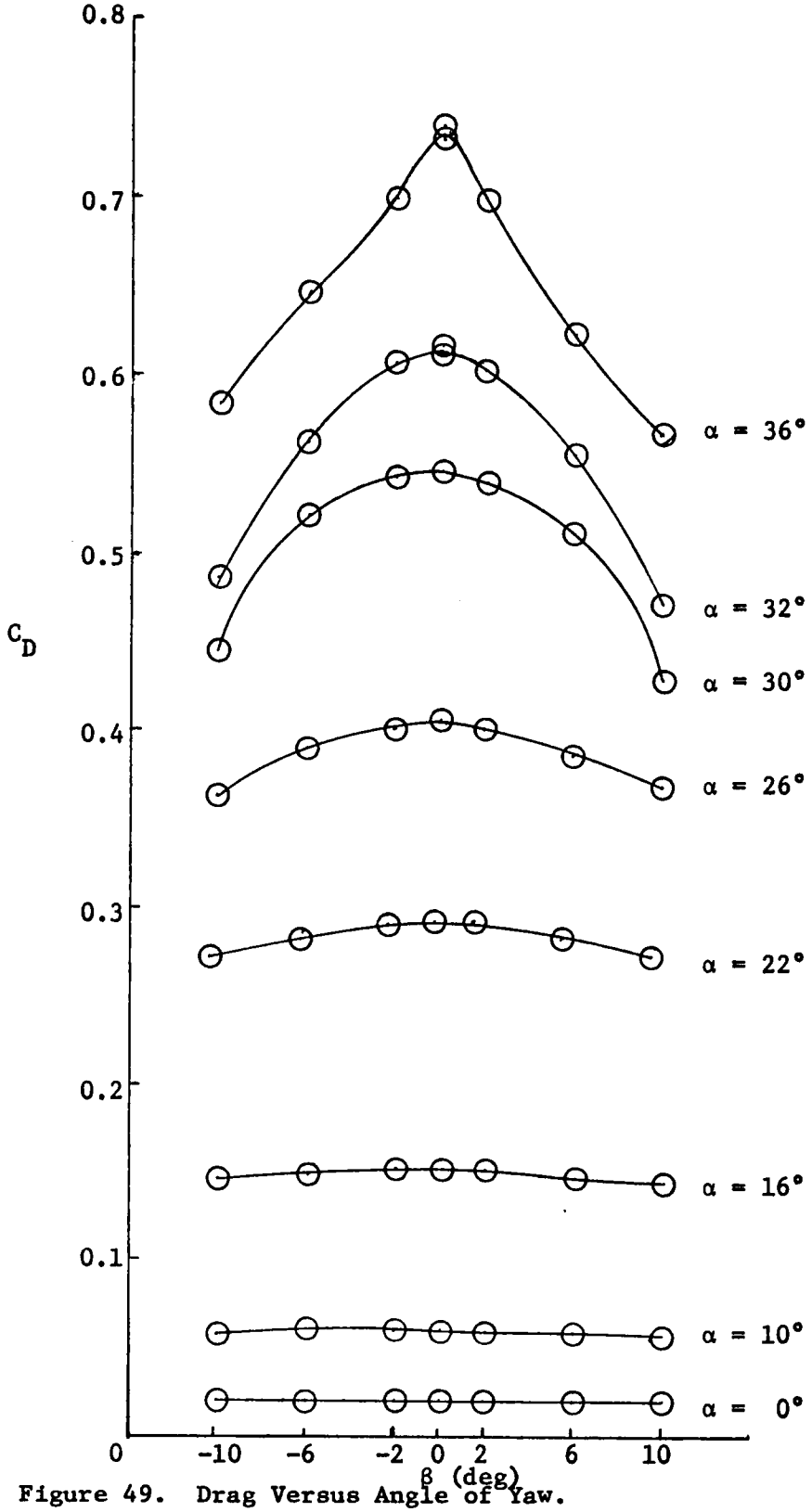

Figure 49. Drag Versus Angle of Yaw.

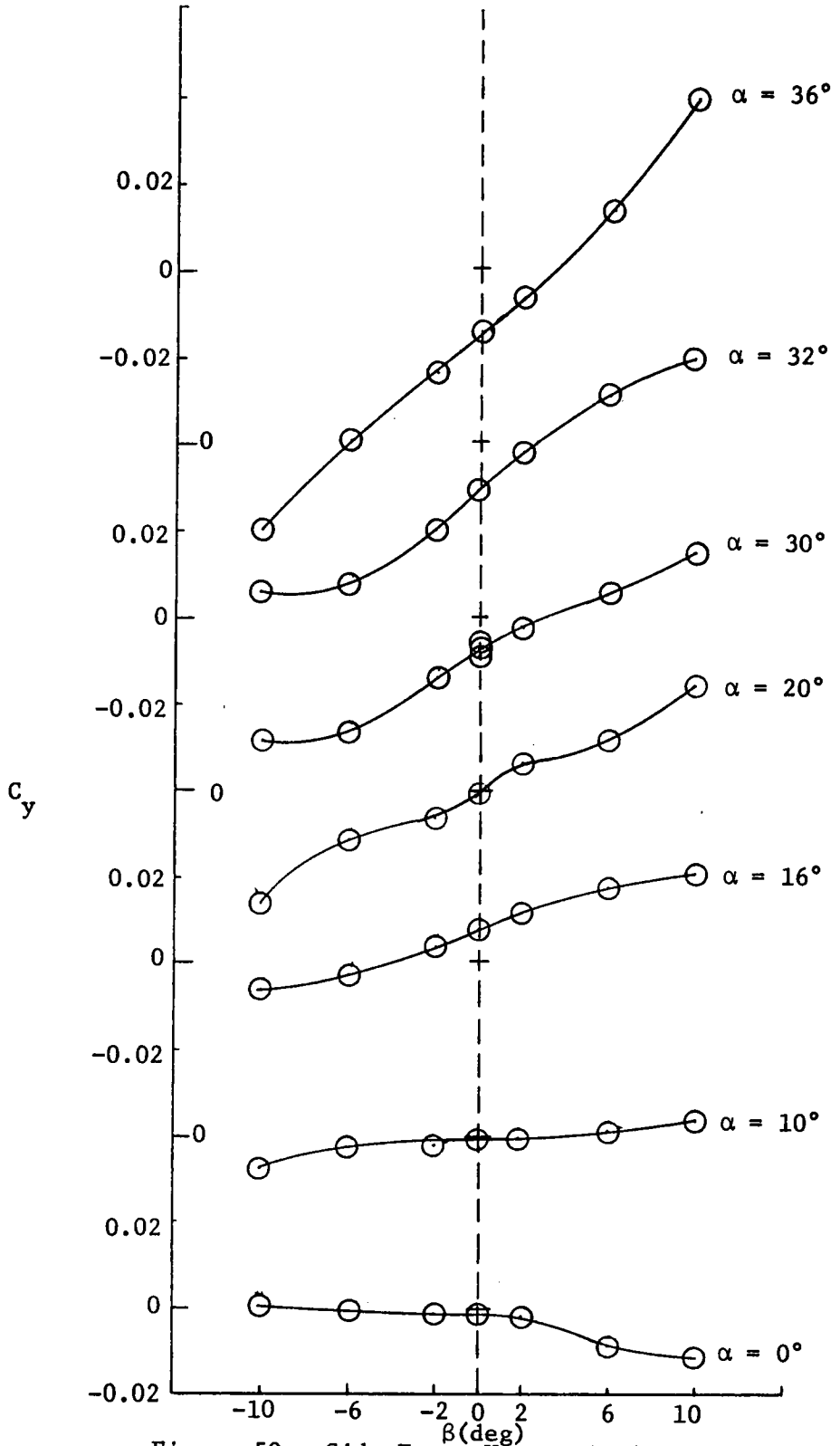

Figure 50. Side Force Versus Angle of Yaw.

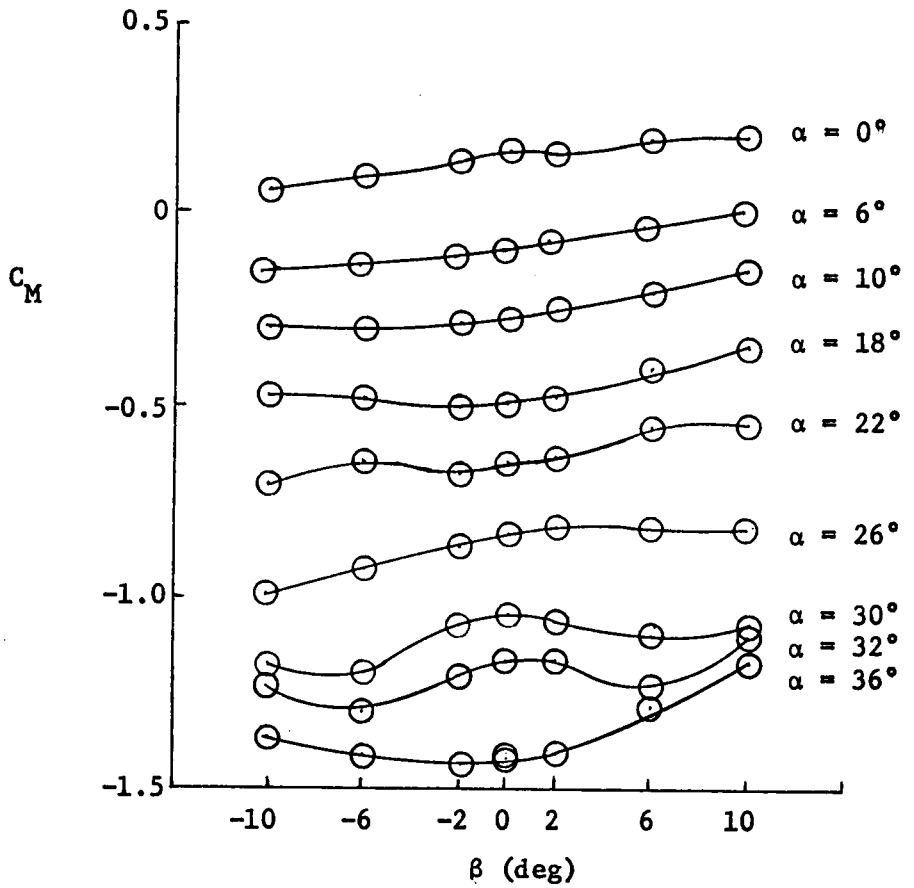

Figure 51. Pitching Moment Versus Angle of Yaw.

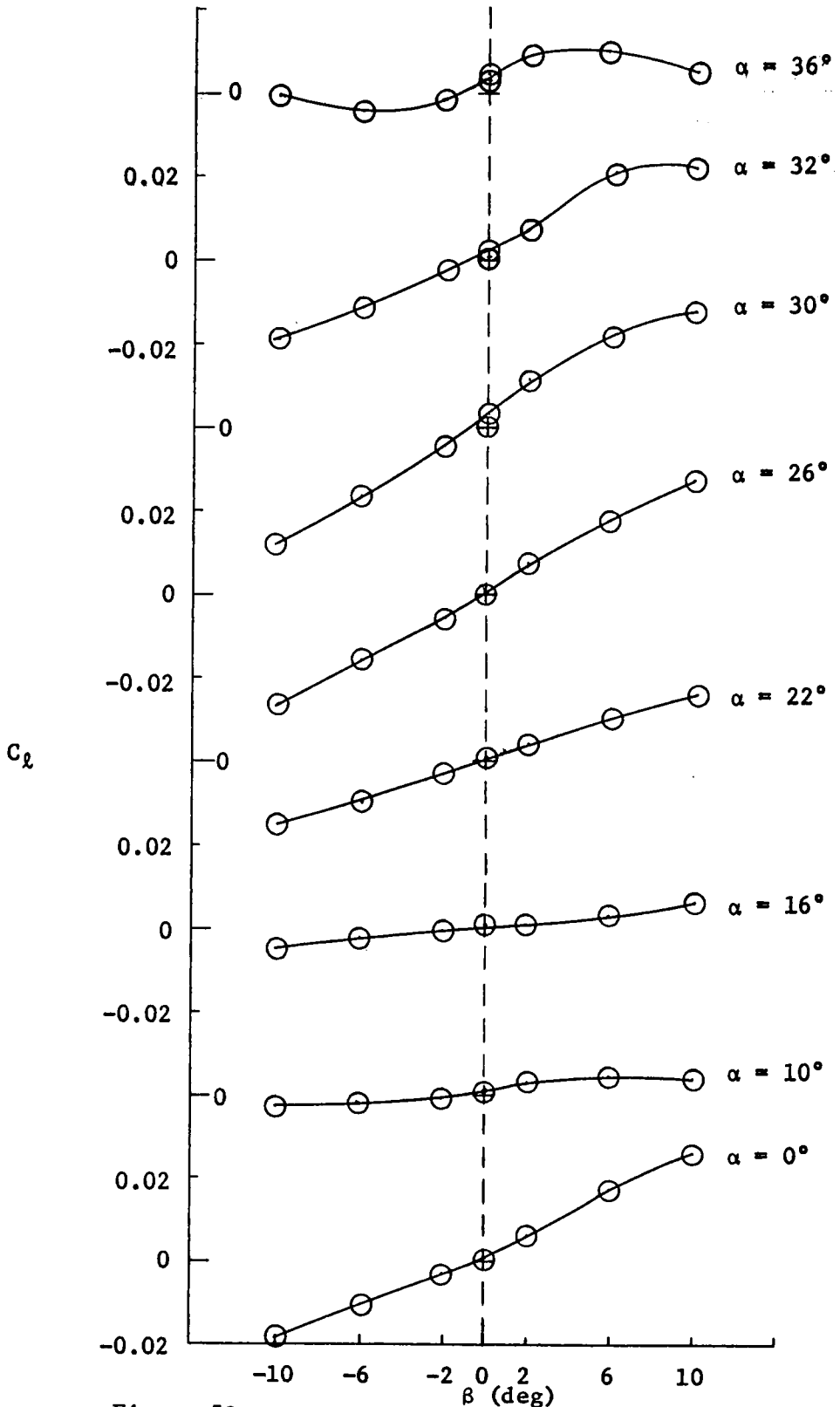

Figure 52. Rolling Moment Versus Angle of Yaw.

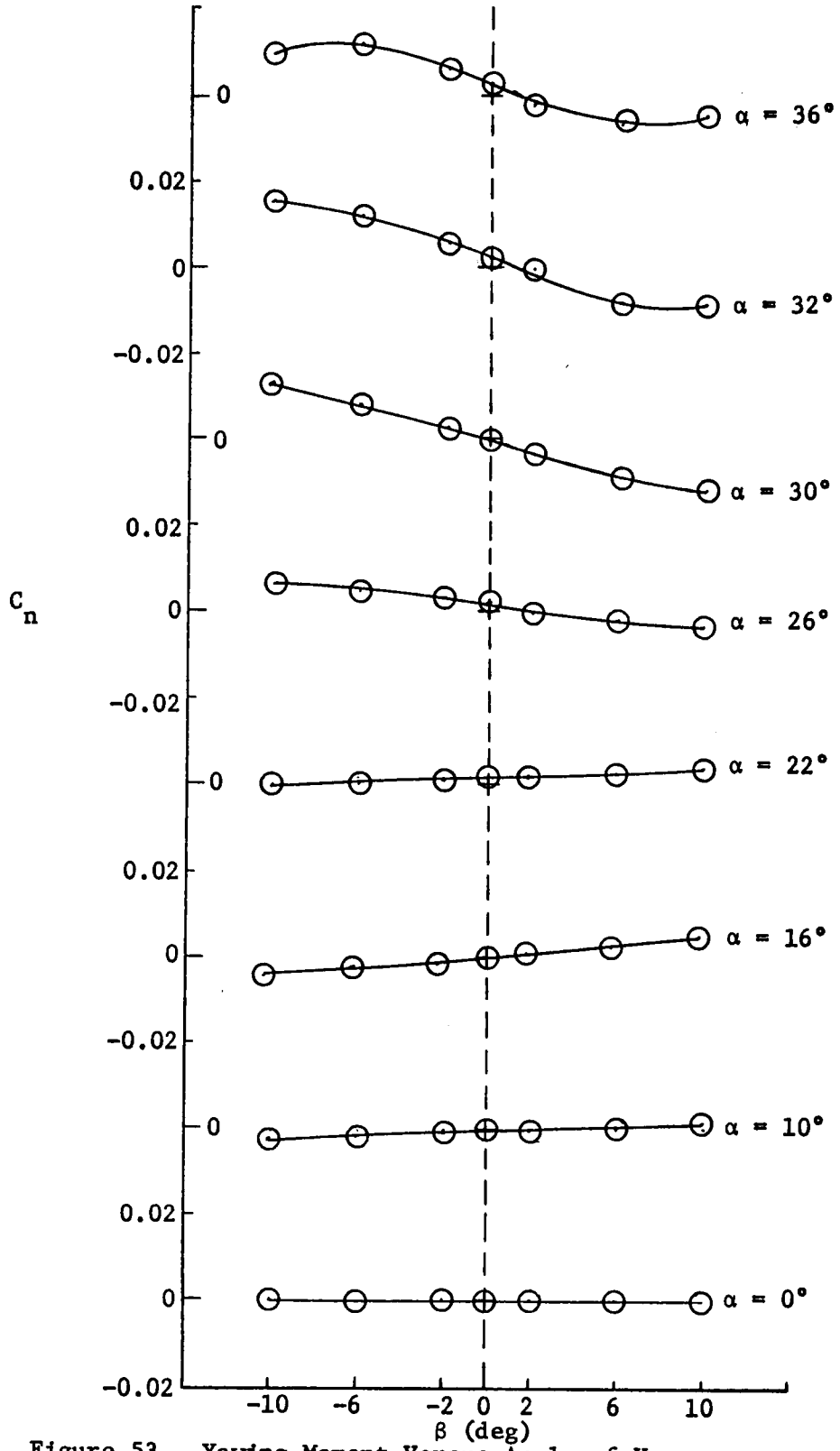

Figure 53. Yawing Moment Versus Angle of Yaw.

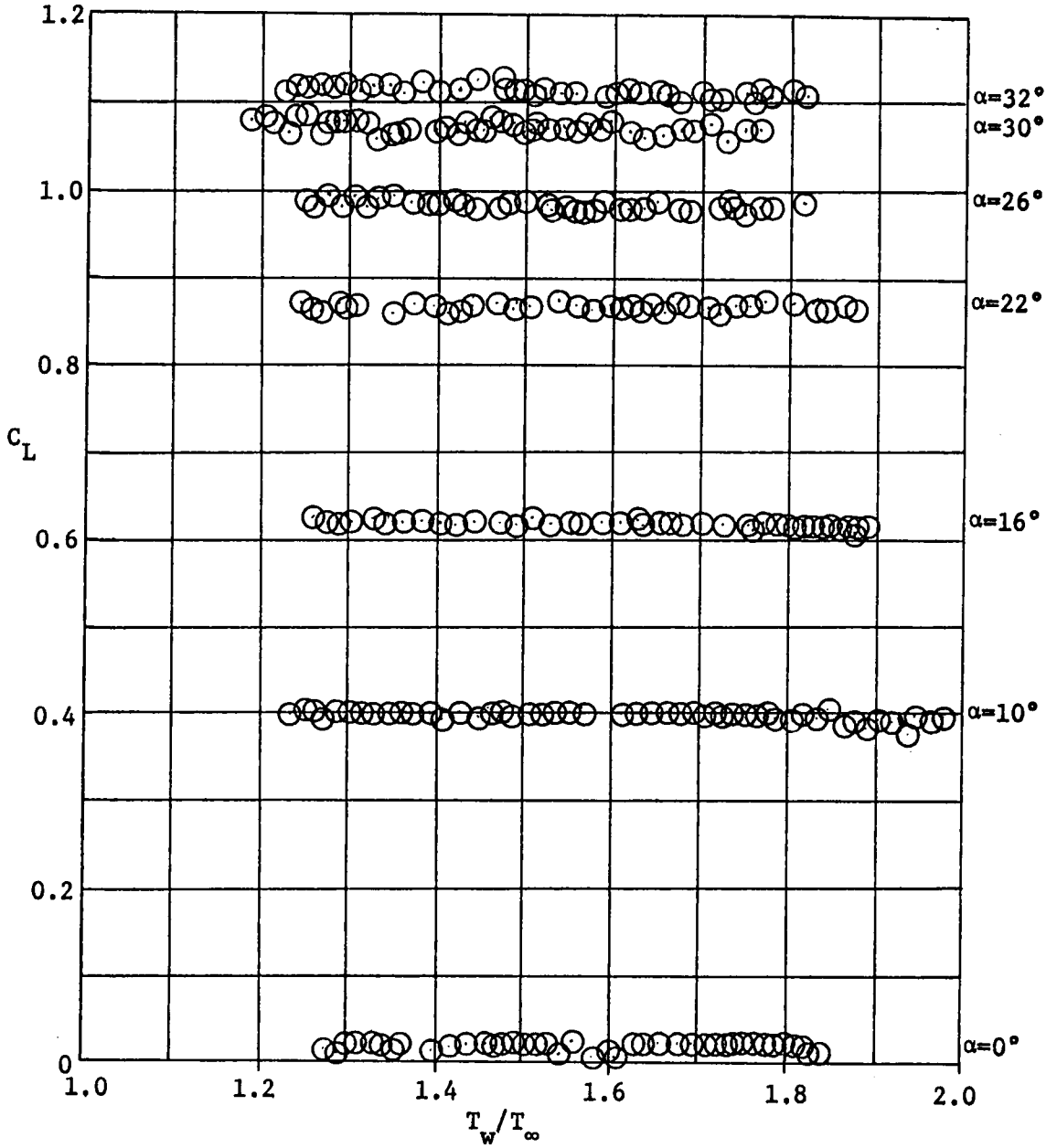

Figure 54. Effect of Surface Temperature on Lift, β = 0°.

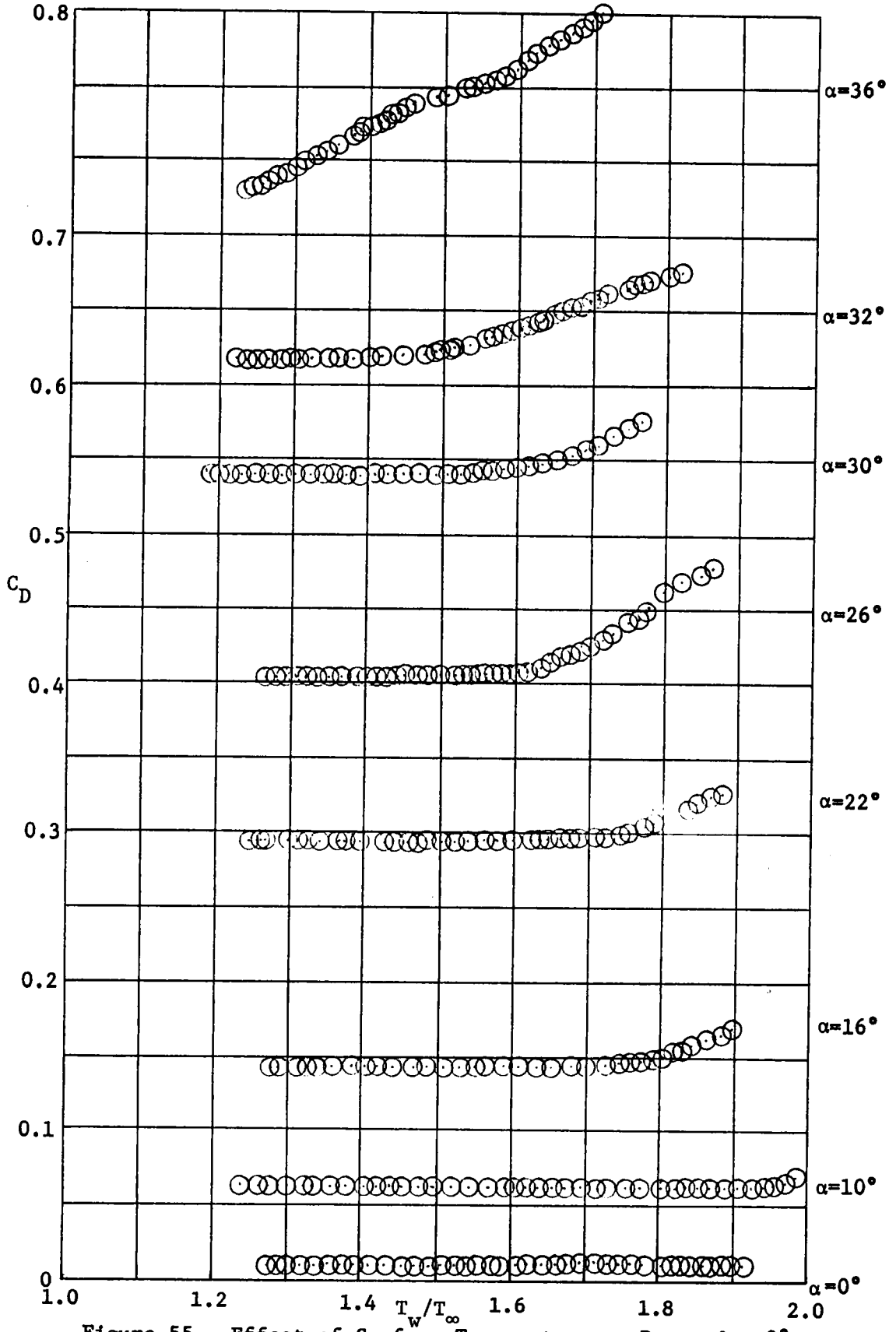

Figure 55. Effect of Surface Temperature on Drag, β = 0°.

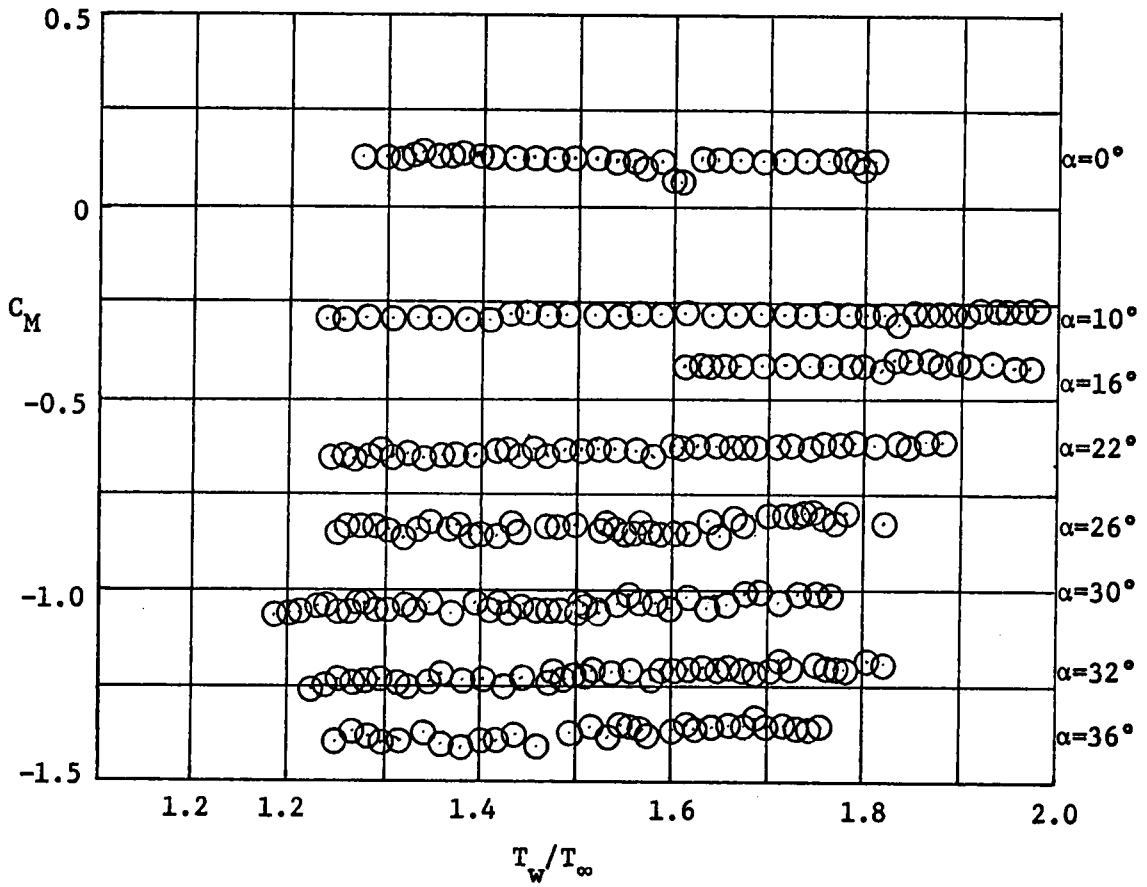

Figure 56. Effect of Surface Temperature on Pitching Moment, β=0°.

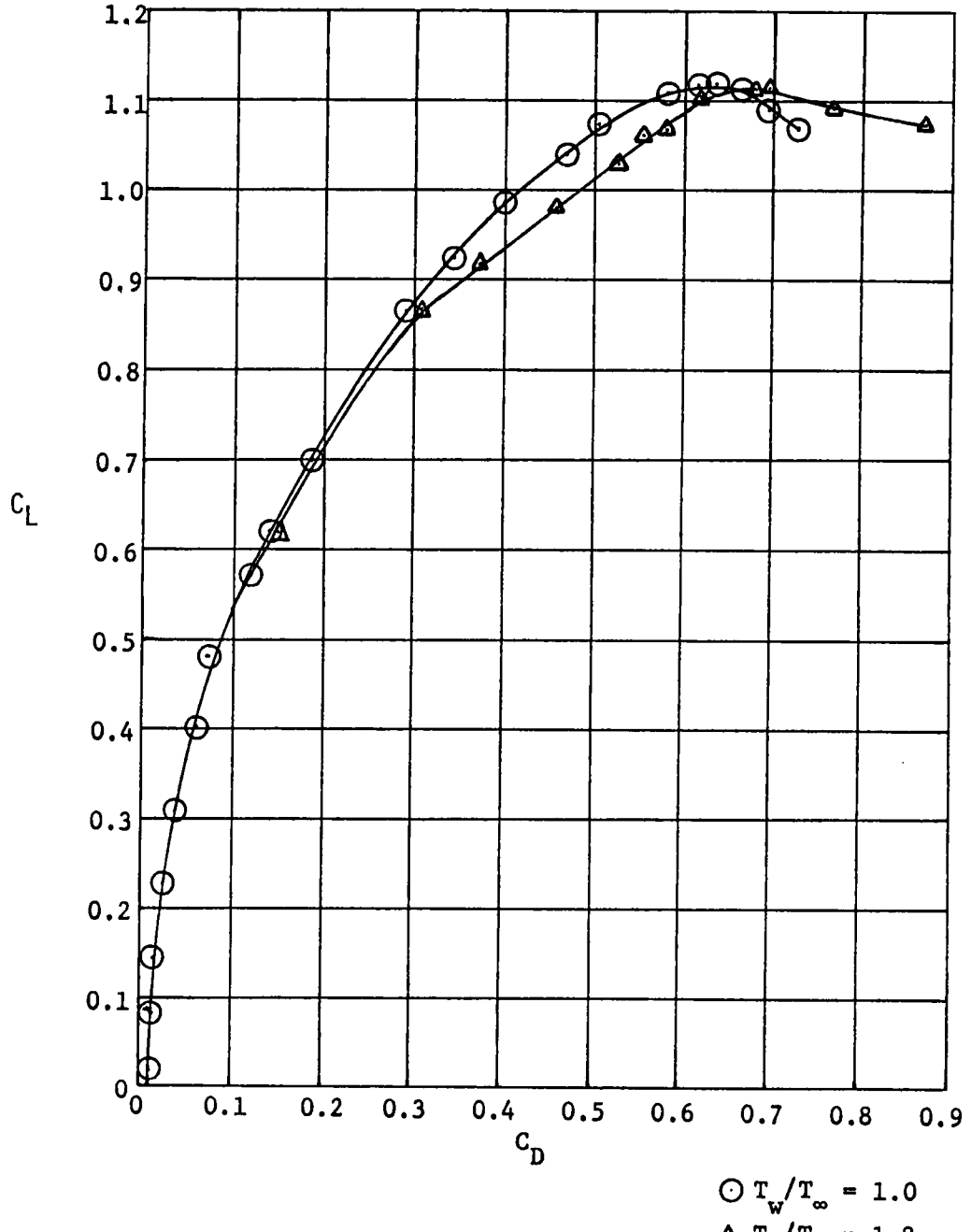

Figure 57. Effect of Surface Temperature on Lift/Drag, Overall View, $\beta = 0°$.

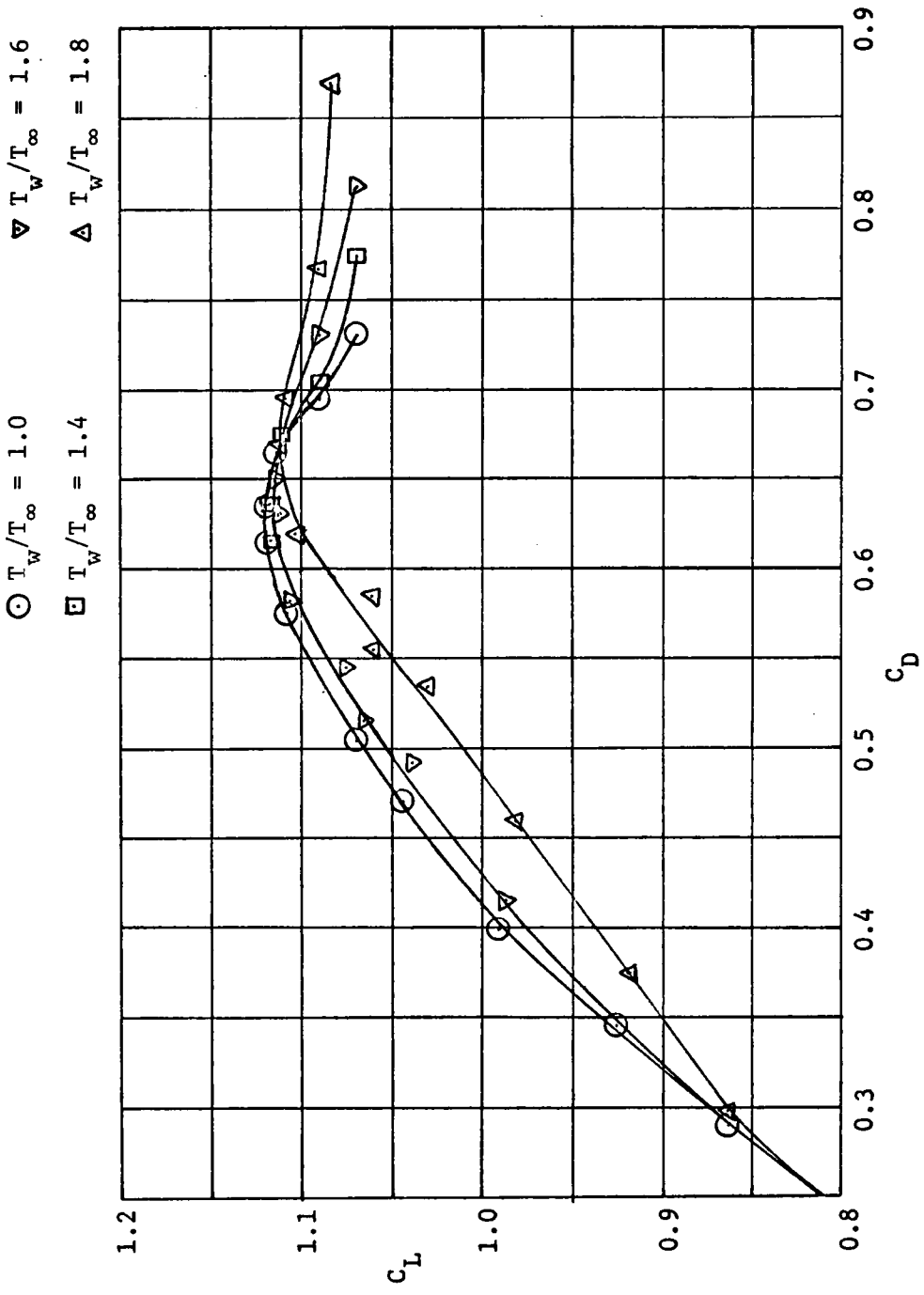

Figure 58. Effect of Surfact Temperature on Lift/Drag, Detail View, $\beta = 0°$.

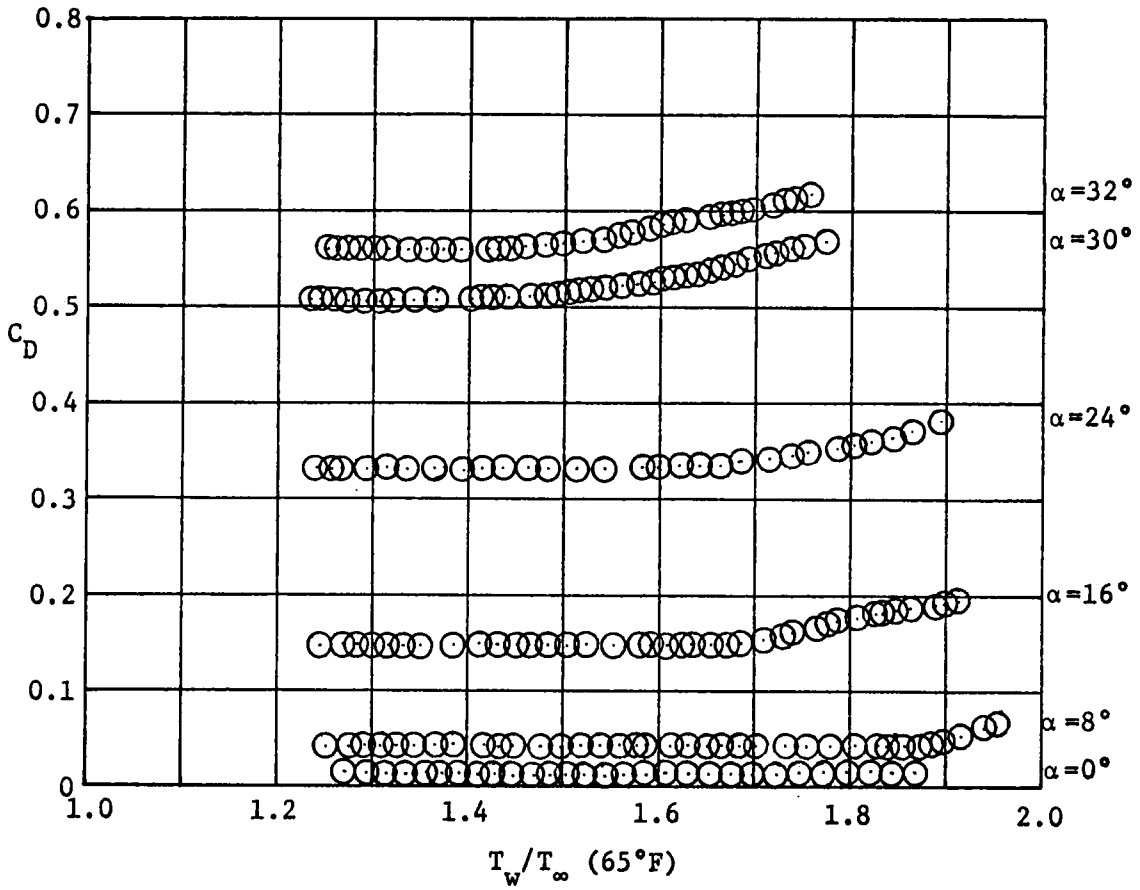

Figure 59. Effect of Surface Temperature on Drag, β = 6°.

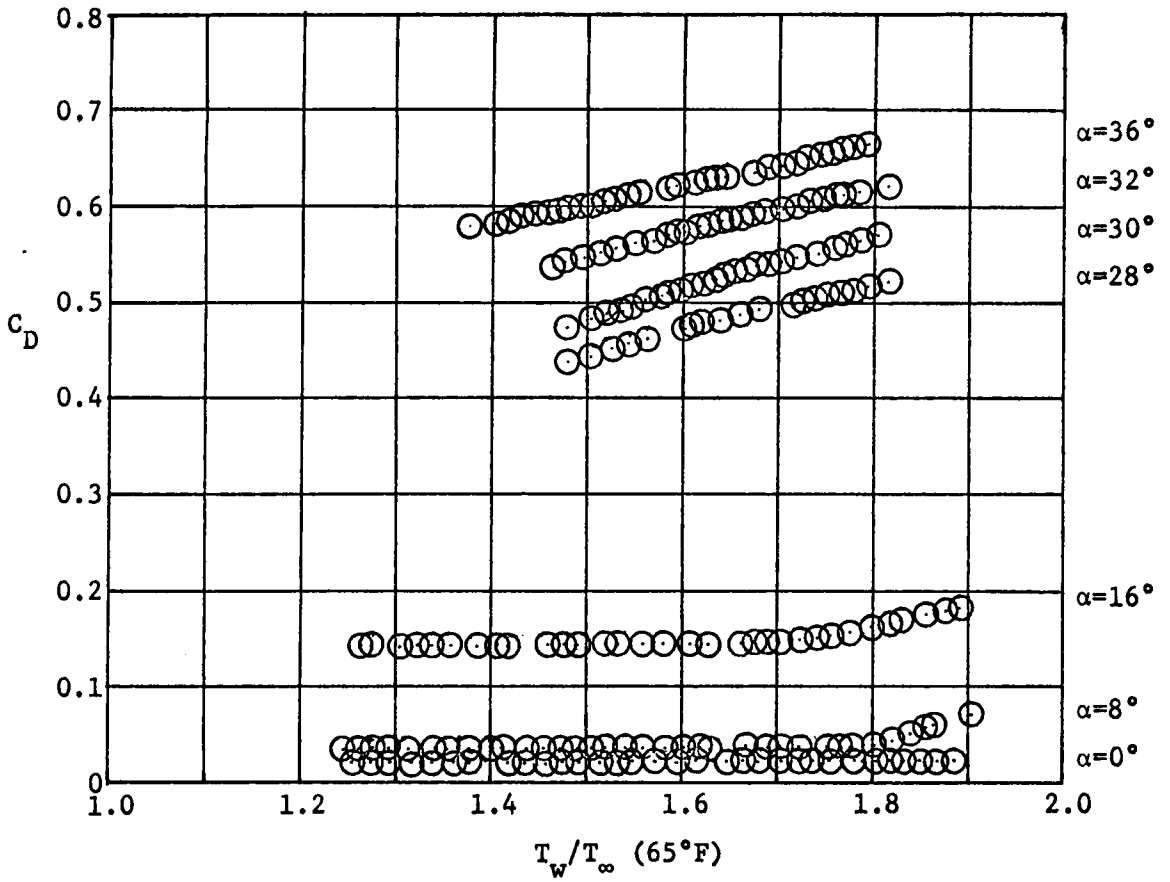

Figure 60. Effect of Surface Temperature on Drag, $\beta = 10°$.

The vita has been removed from the scanned document

HEAT TRANSFER EFFECTS
ON A SUBSONIC DELTA WING

by

Raymond William Blohm, III

(ABSTRACT)

With the advent of the "Space Shuttle" concept, it has become necessary to study the effects of heat transfer on the aerodynamic and boundary layer characteristics of a heated delta wing. Thus, a symmetrical 60° delta wing was tested up to twice freestream temperature in the Virginia Tech 6' x 6' stability wind tunnel. Summaries of the characteristics of the flow over the unheated wing and the theoretical effects of heat transfer are included. It has been found that heat transfer effects on the wing's aerodynamic characteristics are negligible at angles of attack up to one-third of the maximum lift angle. Beyond this, lift and pitching moment show a very small decrease and increase, respectively, up to maximum lift while drag increases 15 per cent to 25 per cent at maximum lift. Further increases in drag occur when the wing is yawed. No decrease in stalling angle of attack with heating is found for all yaw angles.